Chapter 3

Development of an RNA device framework that responds to proteins in human cells

Partially adapted from d'Espaux, L. D., Kennedy, A. B., Vowles, J. V., & Smolke, C. D. (2014). Development of protein-responsive ribozyme switches in eukaryotic cells. In preparation.

Abstract

Synthetic molecular devices for programmable gene regulation in human cells are useful tools for studying biological systems and for developing novel diagnostic and therapeutic platforms. Ribozyme switches are a class of gene-regulatory device that have been designed to exhibit programmable gene regulation activity in response to small molecule ligand inputs; however, response to protein ligands has not been demonstrated to date. We developed ribozyme switches that respond to the bacteriophage MS2 coat protein and demonstrated ligand-responsive modulation of gene expression in a human cell line. We investigated different strategies for device architecture and optimized the protein ligand to maximize sensitivity of the system, demonstrating up to 6.5-fold activation and up to 4.6-fold inhibition of gene expression from the ON and OFF switch platforms, respectively. We also explored the mechanism of action and ligand localization requirements of the ribozyme switch by localizing the protein ligand to different cellular compartments. We found that ligand localization to either the nucleus or the cytoplasm is sufficient for switching activity. Finally, we extended the platform to the design of a ribozyme switch responsive to the endogenous signaling protein β-catenin, demonstrating the ability of our platform to respond to an important disease marker.

Introduction

Synthetic ligand-responsive genetic regulators are important tools for controlling diverse biological systems spanning from engineered microorganisms to human patients. Many small-molecule-responsive RNA-based switches have been demonstrated in eukaryotic systems, but fewer have responded to protein inputs[1]. As changes in protein expression determine cellular phenotype, molecular devices that directly detect and respond to intracellular concentrations of proteins are important engineering tools. Such genetically encoded devices have applications in the noninvasive detection and quantification of proteins in a complex cellular environment, as well as in targeting therapeutic activities to specific diseased cellular states.

Several examples of mammalian gene control platforms have been described that utilize different architectures and gene-regulatory mechanisms. One common strategy is the placement of an aptamer in the 5' untranslated region (UTR) of the gene of interest, such that ligand binding causes translational repression by preventing proper ribosome assembly for initiating translation[2–7]. In one example, binding of tryptophan RNA-binding attenuation protein (TRAP) to its 5' UTR binding site produced 180-fold translational repression[2]. In another example, the archaeal ribosomal protein L7Ae was used to regulate two reporter genes simultaneously[6]. However, this approach is limited to OFF switches unless it is coupled with an additional genetic inverter component[8], and can respond only to cytoplasmic protein ligands. Additionally, in mammalian cells 5' UTR secondary structure can nonspecifically interfere with translation, further limiting this regulatory strategy.

The incorporation of other classes of gene-regulatory elements can further expand the capabilities of these protein-responsive switches. For example, an L7Ae-responsive ON switch was created using a trans-acting regulator RNA that bound to the translation initiation site on the target messenger RNA (mRNA), thereby silencing gene expression[4]. Binding of L7Ae to its aptamer in the regulator RNA prevented binding to the mRNA, thereby derepressing expression of the target gene. As another example, an L7Ae-responsive ON switch based on an RNA interference (RNAi)-based silencing gene-regulatory element was described that incorporated an aptamer in the loop region of the short hairpin RNA (shRNA), such that ligand binding in the cytoplasm masked the Dicer recognition site and prevented processing, inhibiting the gene silencing effect observed with proper Dicer processing in the absence of ligand[9]. In a third example, ON and OFF switches modulating precursor mRNA (pre-mRNA) alternative splicing were used to control the inclusion of an exon containing a premature stop codon in response to endogenous protein disease markers in the nucleus[10].

Protein-responsive translational regulators have also been used to regulate genetic circuits in mammalian cells. In one example, an L7Ae-responsive OFF switch was used to control L7Ae expression in a genetic feedback loop[5]. In another example, that same switch was used in conjunction with an shRNA-based ON switch to precisely regulate the relative expression levels of a proapoptotic and an antiapoptotic gene, thereby controlling cell fate in HeLa cells[9]. In addition, more complex genetic circuitry has been demonstrated by incorporating both protein-responsive translational regulators and small-molecule-responsive transcriptional regulators to engineer genetic systems that perform

digital logic computations and fundamental arithmetic operations on prescribed molecular inputs[3].

One main advantage of post-transcriptional regulators such as those described above relative to transcriptional regulators is that they exhibit a faster change in gene expression in response to changes in the level of protein ligand. When translation of the transcript is hindered or the transcript is degraded, synthesis of the encoded protein ceases, while the product of a transcriptionally silenced gene continues to be translated from existing mRNA. However, generally the components in these regulatory devices are capable of either ON or OFF switching, but not both. Rarely can the components be coupled without disrupting their individual functions, and the devices are generally not portable between microbes and higher eukaryotes. A single gene-regulatory device platform capable of overcoming these limitations would present a more flexible and streamlined design process for devices tailored to different systems.

Ligand-responsive ribozyme switches have been used to regulate gene expression in yeast[11–13] and mammalian cells[14–16]. Ribozyme switches are incorporated into the UTR of the target gene, where ligand-regulated cleavage of the transcript leads to silencing of gene expression[11]. This platform possesses a number of important advantages that many of the protein-responsive devices demonstrated to date in mammalian cells lack. First, ribozyme switches can be programmed to turn gene expression on or off in response to almost any ligand for which there exists an RNA aptamer. Second, switch activity can be tuned through modifications to the sequence of the aptamer, ribozyme, and transmitter components. Third, switch components can be modularly coupled without disrupting their activities. Finally, ribozyme switches are

highly portably between different organisms because their mechanism of action is independent of cell-specific machinery[11,17]. However, one current limitation of ribozyme switches is that the platform has only been demonstrated to respond to small molecule ligands. It is also unknown where in the cell the ribozyme cleavage event occurs. A protein-responsive ribozyme switch platform would leverage the important design advantages of the existing small-molecule-responsive platform while expanding its capability to process a new and important class of inputs.

We describe the development of a protein-responsive ribozyme switch platform for regulating gene expression in mammalian cells. We investigated a variety of device architectures, expanding beyond the design of the small-molecule responsive ribozyme switches, using an aptamer for the bacteriophage MS2 coat protein and controlling the expression of a fluorescent reporter gene. We developed and optimized a genetic expression system for quantitative characterization of device activity in human cells. The most highly active switch designs exhibited up to 6.5-fold activation and up to 4.6-fold inhibition of gene expression from the ON and OFF switch architectures, respectively. Experiments examining the impact of ligand localization on device activity indicated that the ribozyme switch platform is uniquely flexible in responding to ligands in either the nucleus or the cytoplasm. Finally, we describe attempts to develop ribozyme switches responsive to other proteins and demonstrate a device responsive to the endogenous signaling protein β-catenin.

Results

Design of protein-responsive ribozyme switch platforms

While previous work in the Smolke laboratory has demonstrated ligand-responsive ribozyme switches, these studies have been limited to small molecule ligands[11]. In developing protein-responsive ribozyme switch platforms we focused our initial designs on integration strategies for an aptamer to the bacteriophage MS2 coat protein (sensor) and the satellite RNA of tobacco ringspot virus (sTRSV) hammerhead ribozyme (actuator). The MS2 protein and its natural stem-loop aptamer were selected as the initial ligand-aptamer pair for this study as they have been extensively used in cellular systems[2,3,6,18–22] and as MS2 is a heterologous protein its levels can be readily controlled. Using this sensor and actuator we explored different design strategies for coupling these components in a way that would enable the binding of the protein ligand to affect the activity of the hammerhead ribozyme.

The simplest design we explored was the direct-coupled architecture, in which the MS2 aptamer is directly coupled to either loop I or loop II of the hammerhead ribozyme (Figure 3.1, MS2-A), without any separate transmitter component linking the sensor and the actuator as incorporated in other small-molecule-responsive ribozyme switch platforms[11]. We designed two different aptamer integration points in each of the loops, and we varied the loop I sequence. The hypothesis underlying the direct-coupled architecture is that the relatively large size of the protein ligand MS2 would disrupt the ability of the ribozyme to fold into the catalytically-active three-dimensional structure, sterically interfering with the tertiary interactions between loops I and II that have been shown to be necessary for cleavage activity at physiological Mg^{2+} concentrations[23]. The

direct-coupled architecture obviates the need to design the ribozyme switch to adopt distinct cleavage-active and cleavage-inactive conformations, and thus is a simpler design than strategies that incorporate directed secondary structure rearrangements. However, it is possible that this design may be more dependent on the size of the protein ligand and the orientation by which the protein ligand binds to its aptamer.

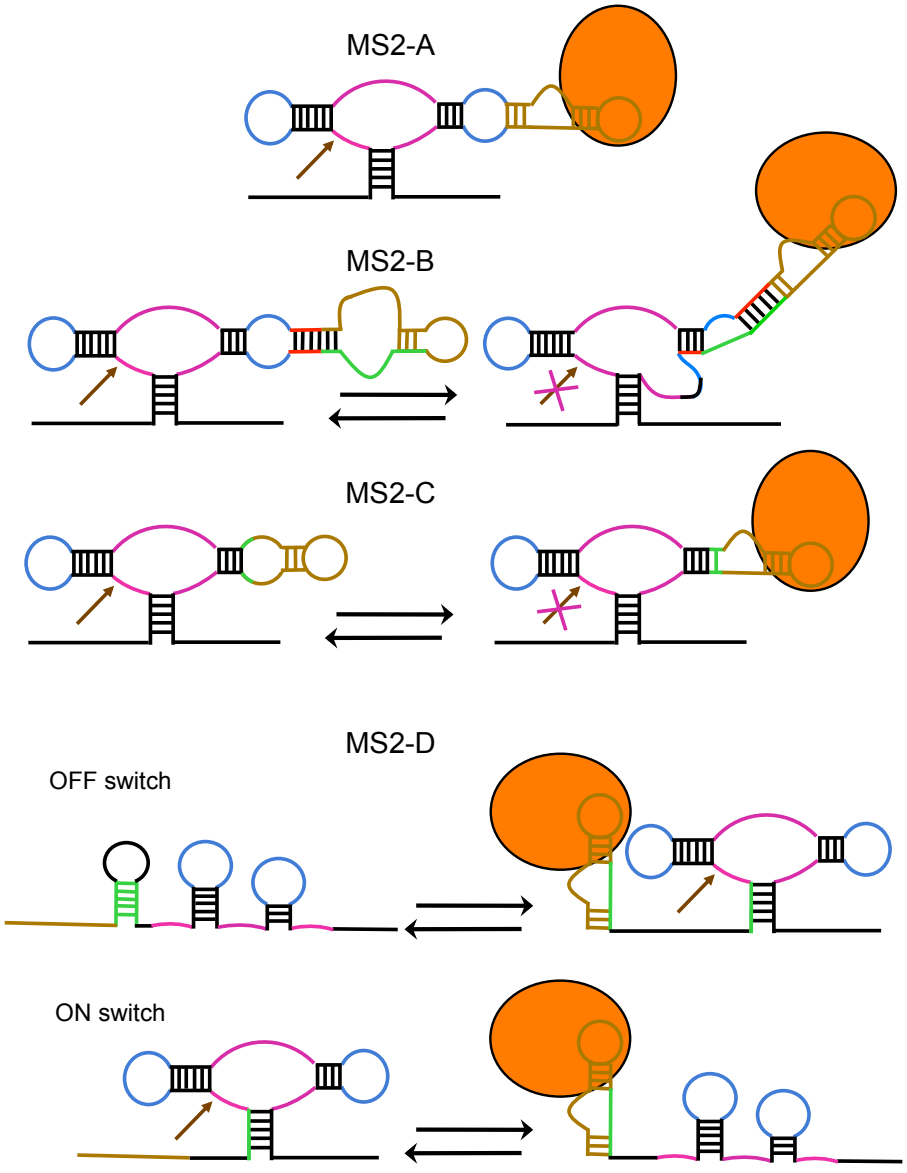

Figure 3.1. MS2-responsive ribozyme switch designs. MS2-A: The MS2 aptamer is coupled directly to the loop. MS2-B: The MS2 aptamer is coupled through a transmitter affecting the secondary structure of stem II and the catalytic core. MS2-C: The MS2 aptamer is coupled through a transmitter affecting the secondary structure of the loop. MS2-D: The MS2 aptamer is placed directly upstream of the ribozyme and a transmitter affecting the formation of stem III. The catalytic core is shown in magenta, loops and bulges are shown in blue, stems are shown in black, the transmitter is shown in green and red, the aptamer is shown in brown, and the MS2 ligand is shown in orange. The cleavage site is indicated with an arrow. See Supplementary Table 3.1 for sequences.

We designed three additional ribozyme switch platforms that incorporated directed secondary structure rearrangements into distinct cleavage-active and cleavage inactive conformations. The first set of ribozyme switches contains a transmitter designed to alter the secondary structure of one of the stems and the catalytic core (Figure 3.1, MS2-B). These ribozyme switches employ the same design strategy as previously developed small-molecule-responsive devices[11], with sequence variations in loop I, the transmitter, and the aptamer. The next set of designs contains a loop-transmitter that alters the secondary structure of the loop to which the aptamer is attached (Figure 3.1, MS2-C), which is expected to disrupt important tertiary interactions with the other loop. We designed an OFF switch, MS2-C1, in which the aptamer and loop-transmitter are integrated into loop I, and three ON switches with varied loop I sequences in which the aptamer and loop-transmitter are integrated into loop II. In the final set of designs, the aptamer is not incorporated into the ribozyme, but is instead placed immediately

upstream in a sequential fashion (Figure 3.1, MS2-D). Alternate hybridization between the aptamer stem and stem III of the ribozyme prevents the aptamer and ribozyme from folding simultaneously in ON switches, while OFF switches contain a competing hairpin that prevents the folding of the aptamer and ribozyme, unless ligand binding stabilizes the aptamer and prevents the competing hairpin from folding. These six designs varied in the length and sequence identity of the transmitter component.

Initial characterization of protein-responsive ribozyme switches in a human cell line

The MS2-responsive ribozyme switch designs were tested for gene-regulatory and ligand-responsive activity in a human cell line. The initial characterization construct was based on the ribozyme switch regulating a green fluorescent protein (GFP) reporter protein and measuring fluorescence under different MS2 levels through a flow cytometry assay. Briefly, the ribozyme switches were located in the 3' UTR of destabilized enhanced GFP (d2EGFP)[24] expressed from a cytomegalovirus (CMV) promoter (Figure 3.2). A doxycycline-inducible expression cassette for MS2 was located on the same plasmid, in which an MS2-DsRed fusion protein was under the control of a CMV promoter with two tetracycline operator (TetO) sites located downstream of the promoter (CMV-$TetO_2$). The plasmid constructs were transiently transfected into a Flp-In T-REx human embryonic kidney 293 (HEK293) cell line, which stably expresses the tetracycline repressor (TetR). Thus, in the absence of doxycycline transcription of the protein ligand is inhibited by TetR, and transcription is activated by the addition of doxycycline which inhibits TetR binding to the operator sites.

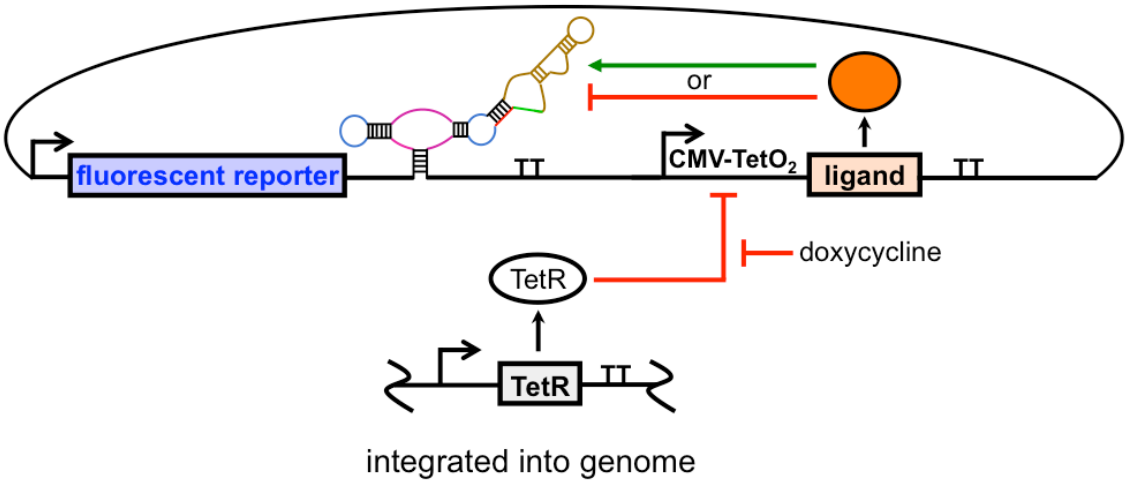

Figure 3.2. Protein-responsive ribozyme switch characterization system. A fluorescent reporter with ribozyme switch and a protein ligand are encoded on a plasmid. A tetracycline-responsive CMV-$TetO_2$ promoter controls expression of the protein ligand and the fluorescent reporter protein is expressed from a constitutive promoter. The plasmid is transiently transfected into a Flp-In T-REx HEK293 cell line, which expresses the TetR repressor. Addition of doxycycline derepresses the CMV-$TetO_2$ promoter, turning on expression of the ligand, which regulates the activity of ON and OFF switches. The plasmid (with both fluorescent reporter and ligand genes) can used in transient transfection assays or stably integrated into the genome for stable expression assays.

We tested four of the direct-coupled designs (MS2-A1, MS2-A2, MS2-A5, and MS2-A6) in the described *in vivo* characterization assay. We selected designs that exhibited the highest *in vitro* cleavage rates in a surface plasmon resonance (SPR) assay (Andrew Kennedy, unpublished results). We found that these ribozyme switch designs were able to downregulate GFP gene expression to varying degrees, but that cleavage activity was not attenuated by MS2 (Figure 3.3). Subsequent *in vitro* switching assays

(Andrew Kennedy, unpublished results) confirmed that although these designs were capable of both cleavage and binding to MS2, ligand binding did not diminish cleavage activity. These results suggest that although MS2 is approximately the same size as the ribozyme switch, binding alone is not sufficient to disrupt tertiary interactions between the loops and thus cleavage activity.

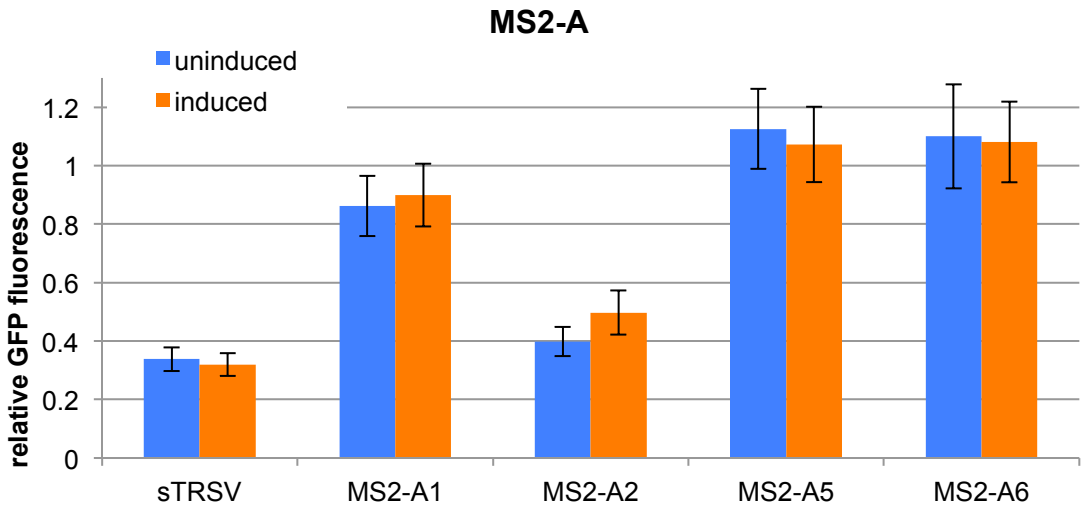

Figure 3.3. Activity of MS2-A designs. Relative GFP fluorescence levels are reported for transiently transfected constructs encoding ribozyme switch sequences. Reported values are geometric mean ± s.d. from biological duplicates and normalized to the absence of ribozyme.

All other ribozyme switch platforms were tested using a slightly modified *in vivo* characterization construct. Specifically, the d2EGFP fluorescent reporter gene was replaced with blue fluorescent protein (BFP), the CMV promoter driving the expression of the reporter gene was replaced with the elongation factor 1 α (EF1α) promoter, and the MS2-DsRed fusion ligand was replaced with MS2 (Figure 3.2). Flow cytometry assays

were performed on a Flp-In T-REx HEK293 cell line transiently transfected with the ribozyme switch constructs. The transmitter designs (MS2-B) showed low to moderate amounts of gene knockdown activity, with three designs, MS2-B2, MS2-B3, and MS2-B7, exhibiting 1.8-, 1.3-, and 1.5-fold, respectively, increases in gene expression in response to doxycycline-induced MS2 (Figure 3.4, MS2-B). MS2-B2 showed the highest switching activity of all designs tested, although its high basal expression level may limit its usefulness in future applications.

One of the loop-transmitter designs (MS2-C) showed low gene knockdown and no switching activity (MS2-C2), while the other three designs responded to MS2 (Figure 3.4, MS2-C). MS2-C3 exhibited a high level of gene knockdown activity, with gene expression almost as low as sTRSV, and the second highest switching activity (1.6-fold increase). MS2-C1 was the only functional OFF switch tested, exhibiting 1.4-fold reduction in gene expression in response to MS2.

The sequential designs (MS2-D) showed the highest levels of gene knockdown activity, with three designs, MS2-D3, MS2-D5, and MS2-D6, exhibiting gene expression as low as sTRSV (Figure 3.4, MS2-D). MS2-D5 showed the highest switching activity (1.5-fold) of the sequential designs.

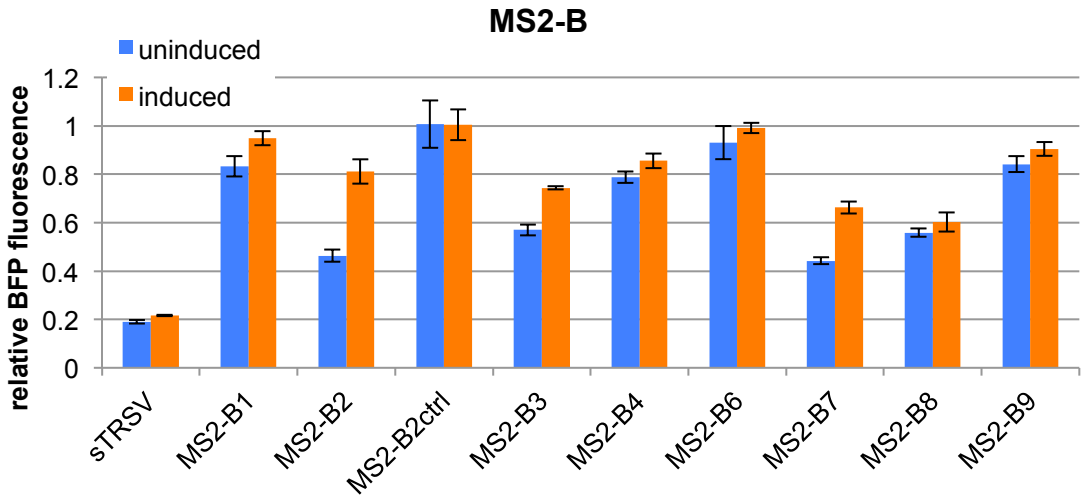
MS2-B
uninduced
induced
relative BFP fluorescence
1.2
1
0.8
0.6
0.4
0.2
0
sTRSV
MS2-B1
MS2-B2
MS2-B2ctrl
MS2-B3
MS2-B4
MS2-B6
MS2-B7
MS2-B8
MS2-B9

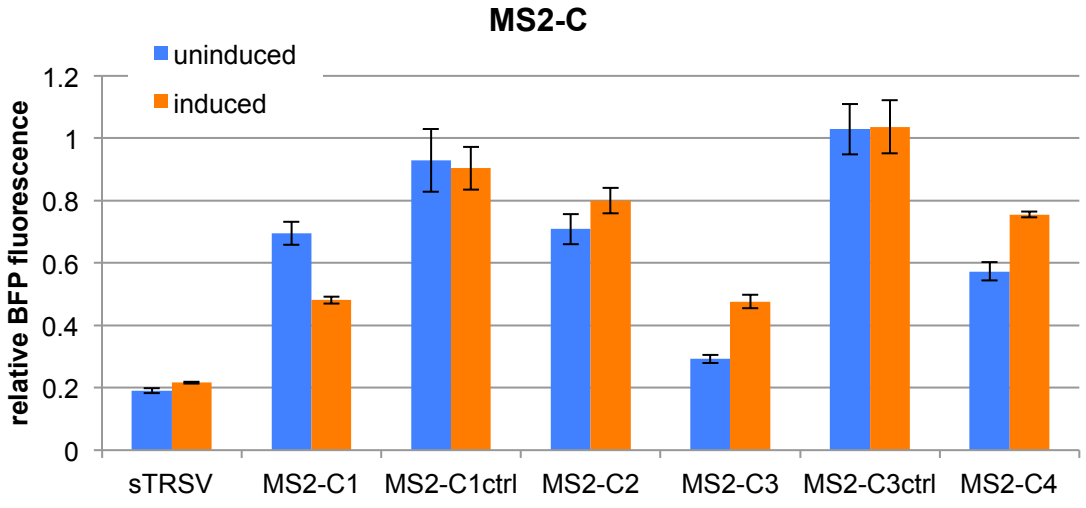
MS2-C
uninduced
induced
relative BFP fluorescence
1.2
1
0.8
0.6
0.4
0.2
0
sTRSV
MS2-C1
MS2-C1ctrl
MS2-C2
MS2-C3
MS2-C3ctrl
MS2-C4

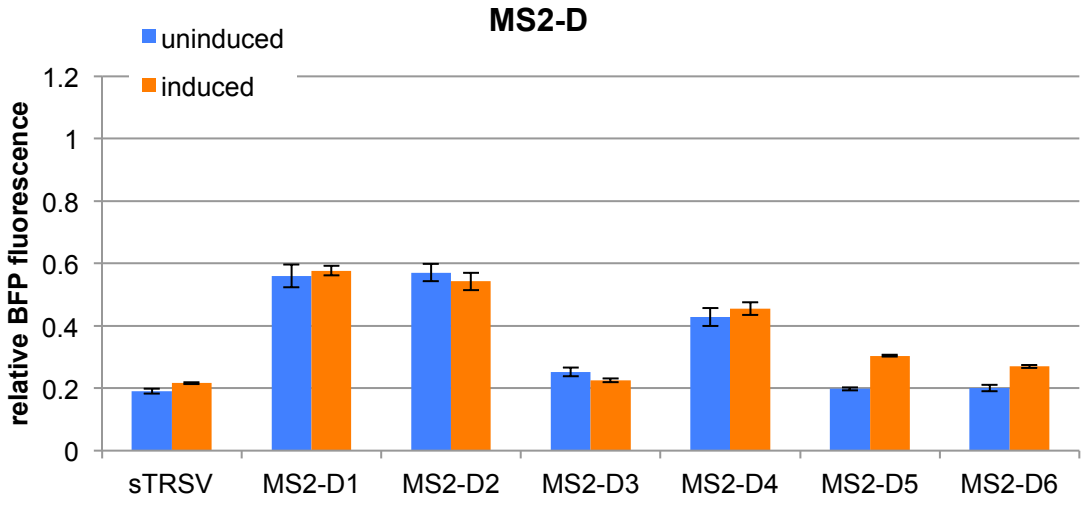
MS2-D
uninduced
induced
relative BFP fluorescence
1.2
1
0.8
0.6
0.4
0.2
0
sTRSV
MS2-D1
MS2-D2
MS2-D3
MS2-D4
MS2-D5
MS2-D6

Figure 3.4. Activity of MS2-B, MS2-C, and MS2-D designs. Relative BFP fluorescence levels are reported for transiently transfected constructs encoding ribozyme switch sequences. Reported values are geometric mean ± s.d. from biological duplicates and normalized to the non-cleaving sTRSVctrl.

Non-cleaving control versions of three ribozyme switches (MS2-B2ctrl, MS2-C1ctrl, and MS2-C3ctrl) were constructed and tested under identical assay conditions. The control designs did not exhibit gene knockdown activity or responsiveness to MS2 (Figure 3.4). These results indicate that gene knockdown is due to ribozyme cleavage rather than to an effect of device secondary structure alone, and that ligand responsiveness is due to modulation of cleavage rather than an effect of ligand binding alone. Eight designs (MS2-B1, MS2-B2, MS2-B3, MS2-B7, MS2-C1, MS2-C3, MS2-C4, and MS2-D5) were subjected to further testing.

Development of an improved genetic system for quantitative characterization of ribozyme switch activity *in vivo*

In order to more accurately measure the gene-regulatory activity of the protein-responsive ribozyme switches in mammalian cells, we developed and optimized an improved *in vivo* characterization system. As described above, the initial characterization system for the ribozyme switches (Figure 3.2) measured activities through transient transfection assays in order to quickly screen device designs for activity. However, the ease of this screening method is accompanied by a high degree of variability. For example, in a transient assay different cells in the transfected population receive different

amounts of plasmid, such that cells in the transfected population can exhibit a range of gene expression over three orders of magnitude, and a large portion of cells receives no plasmid at all (Figure 3.5). To measure ribozyme switch activity, analysis must be performed on transfected cells only, which was accomplished by gating for cells that expressed a fluorescent protein as a transfection marker. One method that we used to determine the transfected population was to cotransfect a plasmid encoding the expression of a second fluorescent protein with the plasmid encoding a ribozyme switch and its reporter gene. Control experiments in our laboratory have shown that in such cotransfection experiments nearly all transfected cells contain both plasmids (Kathy Wei and Joy Xiang, unpublished results). An alternative method we used to determine the transfected population was to gate transfected cells based on the expression of the reporter gene regulated by the ribozyme switches. While cell populations exhibiting a high level of gene expression are fully distinct from populations of untransfected cells, this is not so for cells expressing devices with high gene silencing activity, with some transfected cells exhibiting similar fluorescence levels as untransfected cells (Figure 3.5). Such devices therefore exhibit an artificially high level of gene expression after gating by this method, as the transfected cells with the lowest gene expression levels have been removed from the analysis. While this effect may result in elevated expression levels for these switches, it does not obscure our ability to observe the switching activity associated with these switches, even for devices with the lowest levels of gene expression (Figure 3.4, MS2-D5 and MS2-D6).

To avoid the variability and efficiency issues inherent in transient transfections, we examined the characterization of constructs that had been stably integrated into the

genome of the cell line as an alternative approach. We used the Flp-In integration system with an HEK293 cell line containing a Flp Recombination Target (FRT) site in its genome. This system allows an expression vector to be integrated into the genome via Flp recombinase-mediated recombination at the FRT site. The resulting isogenic stable cell line presents a homogenous level of gene expression across all cells in the population, although this level is lower than that produced by the same construct when transiently transfected (Figure 3.5). As cells with the desired integration are selected by culturing the transfected cells in selective media, the integration process requires 2–3 weeks to generate isogenic stable cell lines. To ensure maximum flexibility in ribozyme switch characterization, the characterization plasmids were constructed on a backbone that was compatible with both transient transfection and stable integration procedures (Figure 3.2).

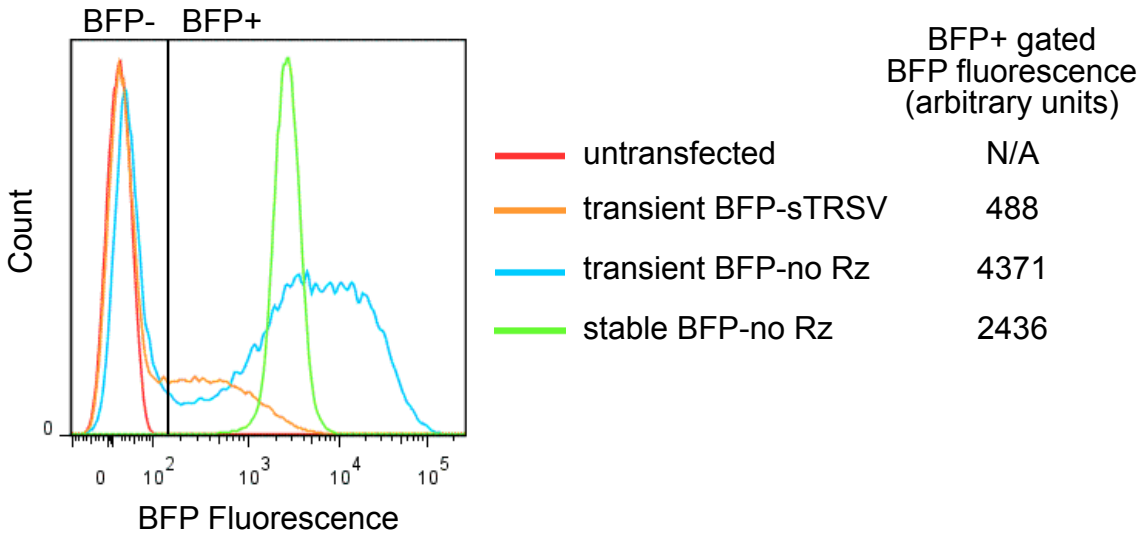

Figure 3.5. Histograms of transiently transfected and stably integrated fluorescent constructs. Transient transfection is not highly efficient and results in a large population

of untransfected cells (red). Gating to remove those cells from analysis also removes a portion of a population of cells expressing a device with a high level of gene silencing (orange). Stable integration of a construct yields a highly homogenous population (green) with lower mean fluorescence than cells transiently transfected with that construct (blue).

As described above, our initial characterization construct utilized a GFP reporter expressed from a CMV promoter to measure the gene-regulatory activity of the ribozyme switches. These constructs encoded a protein ligand expression cassette in which an MS2-DsRed fusion was expressed from a doxycycline-inducible CMV-TetO_2 promoter. We observed that when these constructs were stably integrated into Flp-In T-REx HEK293 cells, the resulting stable cell lines produced no detectable fluorescent signal from the MS2-DsRed fusion in response to doxycycline. In contrast, when using the same constructs in transient transfection assays, doxycycline did elicit a detectable fluorescent signal, albeit low, from the MS2-DsRed fusion. Our control experiments indicated that the expression from the stably integrated constructs were generally lower than that from the same constructs in a transient transfection assay (Figure 3.5). Thus, we concluded that under stable expression conditions the levels of the MS2-DsRed ligand were reduced below the detection threshold of the flow cytometry assay.

To improve characterization of the protein responsiveness of the ribozyme switches in the stable expression assay, we modified the protocol to increase protein ligand levels by transiently transfecting a plasmid encoding the expression of MS2 or the MS2-DsRed fusion into the stable cell lines prior to analysis. However, in the course of

optimizing the protocol for this assay, we noticed two unexpected effects that confounded analysis of the gene-regulatory activity and ligand-responsiveness of the ribozyme switches. First, transient transfection of d2EGFP-expressing cell lines resulted in a population of cells with lower GFP fluorescence levels than untransfected cells, but not as low as parental cells expressing no fluorescent proteins (Figure 3.6A). The appearance of this cell population was observed for transfection of plasmids encoding expression of fluorescent proteins, non-fluorescent proteins, and no proteins (i.e., a plasmid with no mammalian promoters). Transfection of a plasmid encoding a different fluorescent reporter protein, BFP, under the control of a different promoter, EF1α, also led to this effect, ruling out promoter competition as a cause of the knockdown. Importantly, this effect was not observed when an "empty" transient transfection was performed, containing transfection reagent but no plasmid.

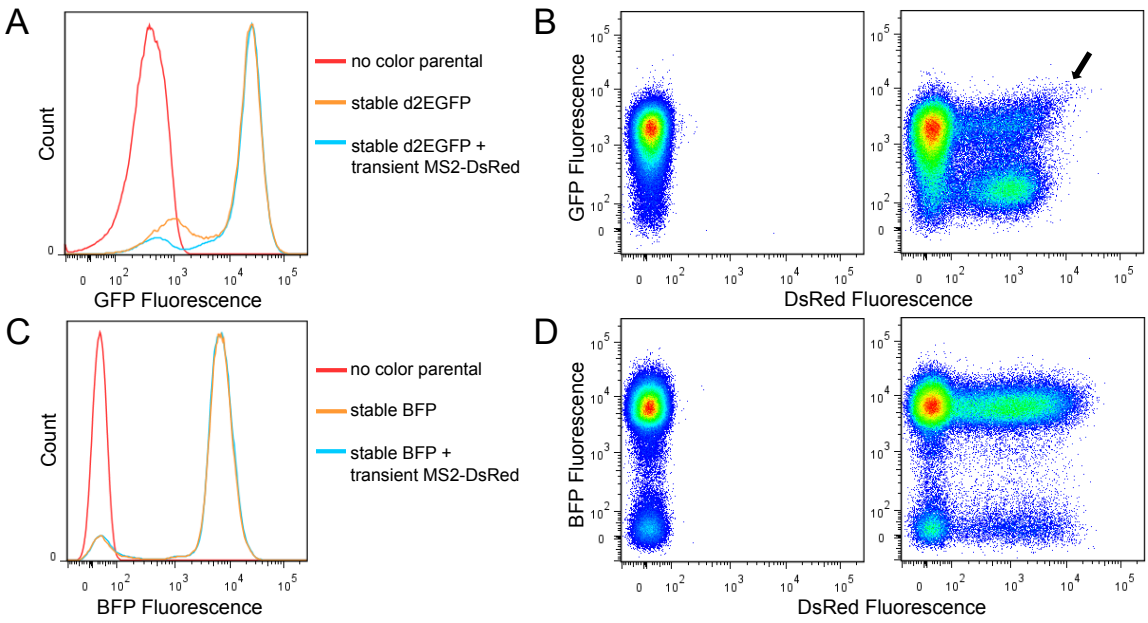

Figure 3.6. Effects of transient transfection of stable cell lines expressing a fluorescent reporter protein. (**A**) Histograms of a d2EGFP stable cell line (blue), that stable line transfected with a plasmid encoding MS2-DsRed (orange), and the no color parental cell line (red). (**B**) Two color scatter plots of a d2EGFP stable cell line, showing the small population of cells (arrow) transfected with a plasmid encoding MS2-DsRed that exhibit higher GFP fluorescence than the stable line itself. (**C**) Histograms of a BFP stable cell line (blue), that stable line transfected with a plasmid encoding MS2-DsRed (orange), and the no color parental cell line (red). (**D**) Two color scatter plots of a BFP stable cell line transfected with a plasmid encoding MS2-DsRed.

The second confounding effect resulting from transient transfection of plasmids encoding MS2-DsRed into the cell lines stably expressing d2EGFP was an increase in GFP fluorescence in cells with the highest DsRed fluorescence to levels higher than the untransfected cell population (Figure 3.6B). Such an effect can be expected from spillover between fluorescence channels due to overlap of the fluorescent protein emission spectra; however, compensation is generally performed to correct for such effects. In this case, the effect remained after proper compensation, and even after over-compensation, suggesting that it is not due to spillover between fluorescence channels. This effect is especially problematic as it is similar to the changes we would expect to observe in GFP fluorescence as a result of the gene-regulatory activity of an MS2-responsive ribozyme switch, with ligand binding to the ribozyme switch preventing cleavage and thereby increasing gene expression. However, the effect was also observed with plasmids encoding DsRed without the MS2 ligand, and in stable lines that did not

contain a ribozyme switch. We therefore concluded that the increase in GFP fluorescence was not a result of ribozyme switch activity.

To address both of these problems, we redesigned our characterization system such that the ribozyme switches were placed in the 3' UTR of BFP, which was under the control of an EF1α promoter. Stable cell lines expressing BFP did not exhibit nonspecific knockdown or fluorescence increases as a result of transient transfection of plasmids, including plasmids encoding the MS2-DsRed fusion (Figure 3.6C and D). This redesigned and optimized characterization system was used for all subsequent ribozyme switch characterization assays, including investigations of the transmitter designs (MS2-B), the loop-transmitter designs (MS2-C), and the sequential designs (MS2-D).

MS2 variants result in optimization of switch sensitivity to ligand

In our initial screening we observed a moderate amount of switching activity from a subset of our MS2-responsive ribozyme switch designs. We next examined whether we could improve ligand sensitivity, and thus switching activity, of these designs by optimizing the ligand itself. MS2 binds to its aptamer in the dimerized form[25]. However, once bound the wild-type protein will multimerize to form a capsid[26]. We hypothesized that multimerization of the ligand could negatively impact switching activity. Thus, we examined two alternative versions of the MS2 ligand: (i) a mutant form of MS2 (MS2mut) containing two amino acid substitutions (V75E and A81G) that is deficient in capsid formation but retains the RNA binding affinity of the wild-type protein[27] and (ii) a fused dimer of the MS2 mutant (2MS2mut). The dimer forms in a head-to-tail orientation, and the fused dimer joins the N- and C-termini together with the deletion of 3

amino acids at the junction. A similar fused dimer without the V75E/A81G substitutions has been shown to retain the same RNA binding affinity as wild-type[28].

We assayed a subset of ribozyme switch designs for sensitivity to these MS2 variants using the improved characterization system (Figure 3.2). We tested the subset of designs that responded to MS2 in our initial screening experiments, as well as MS2-B1 because it showed substantial switching activity in yeast assays (Leopold d'Espaux, unpublished results). We performed the assay using transient expression, similar to our initial experiments with the MS2-B, MS2-C, and MS2-D designs, with MS2mut or 2MS2mut replacing MS2 on the plasmid. Our results indicate that although device basal levels remained mostly unaffected by the change in ligand (as expected), all switches tested were equally or more responsive to MS2mut than MS2 (Figure 3.7A). In addition, most of the switch designs exhibited even greater sensitivity to the 2MS2mut ligand, including MS2-B1, which showed no response to MS2 or MS2mut under identical assay conditions. These results indicate that preventing ligand multimerization is beneficial for switch sensitivity. The increase in sensitivity to 2MS2mut is likely due to increased effective ligand concentration. As the MS2 monomer must dimerize in order to bind to the aptamer[25], expressing the protein as a fused dimer roughly doubles the effective concentration of the ligand.

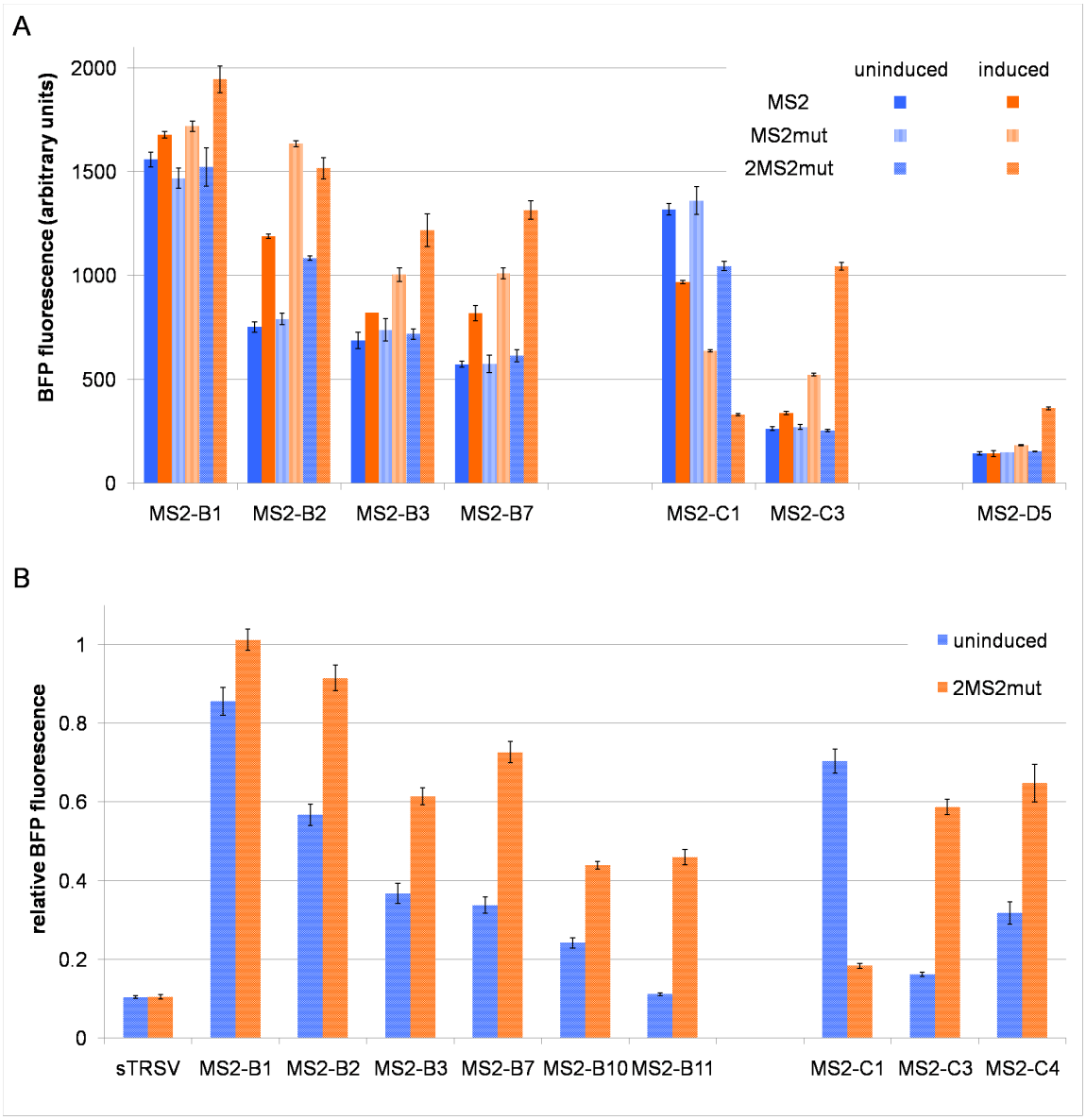

Figure 3.7. Activity of ribozyme switches with optimized ligands. (**A**) Switch response to wild-type MS2, MS2 V75E/A81G (MS2mut), and the fused dimer of MS2mut (2MS2mut). BFP fluorescence levels are reported for transiently transfected constructs encoding ribozyme switch sequences. Reported values are geometric mean ± s.d. from biological duplicates. (**B**) Switch response to 2MS2mut, including two new switch designs. Relative BFP fluorescence levels are reported for transiently transfected constructs encoding ribozyme switch sequences cotransfected with a transfection control

plasmid. Reported values are geometric mean ± s.d. from biological duplicates and normalized to the non-cleaving sTRSVctrl.

We used the results from this assay and our optimized ligand to further explore improvements to the ribozyme switch designs. MS2-B2 differs from MS2-B1 in the sequence of loop I, and we hypothesized that this difference may be the cause of the increased gene knockdown and switching activities observed for MS2-B2. We modified the designs of MS2-B3 and MS2-B7 by changing their loop I sequences to that of MS2-B2, generating MS2-B10 and MS2-B11, respectively. We assayed these new designs with our optimized ligand 2MS2mut (Figure 3.7B). MS2-B11 exhibited the greatest response to ligand (4.1-fold), while the OFF switch MS2-C1 exhibited 3.8-fold switching.

Protein ligand localization allows probing of ribozyme switch mechanism of action

We next investigated how the subcellular localization of ligand affected ribozyme switch activity. For ribozyme switches responsive to small molecules previously developed in the Smolke laboratory[11] it is expected that the ligand will freely diffuse throughout the cell, available to bind to its aptamer over the entire lifetime of the mRNA, from transcription in the nucleus to translation in the cytoplasm. Proteins, however, are commonly localized to specific subcellular locations. Localization of the protein ligand enables the investigation of where in the cell the ribozyme cleaves, and consequently when it cleaves relative to mRNA nuclear export and translation. In the case of an ON switch, where ligand binding is required to prevent ribozyme cleavage, the ribozyme

switch may be unresponsive if the ligand is localized to one cellular compartment. If the protein is localized to the cytoplasm the ribozyme may cleave in the nucleus during or immediately following transcription, and if the protein is localized to the nucleus the ribozyme may cleave after export to the cytoplasm. We attempted to elucidate the ligand localization requirements of our MS2-responsive switches in order to discover where in the cell the ribozyme cleaves, which in turn will inform the choice of new protein ligands for ribozyme switches in the future.

For all experiments described above, we expected the ligand to be found in both the nucleus and the cytoplasm, as MS2 (14 kDa), MS2mut (14 kDa), and 2MS2mut (28 kDa) are small enough to passively diffuse through the nuclear pore without the aid of any nuclear transport machinery[29]. We attempted to control protein localization by creating 2MS2mut constructs with either an N-terminal nuclear localization sequence derived from Simian virus 40 (SV40)[30] (NLS-2MS2mut) or a C-terminal nuclear export sequence derived from protein kinase A inhibitor α (PKIα)[31] (2MS2mut-NES). We transiently transfected Flp-In T-REx HEK293 cells with plasmids encoding each of these three 2MS2mut localization variants, induced protein ligand expression from the CMV-$TetO_2$ promoter using doxycycline, and harvested the total protein in nuclear and cytoplasmic extractions. Immunoblotting of these extracts with an antibody specific for MS2 revealed that 80% of an average cell's 2MS2mut is found in the cytoplasm, despite its small size (Figure 3.8A). The NES tag localized 90% of an average cell's 2MS2mut to the cytoplasm, which is comparable to the distribution of the cytoplasmic control protein. Compared to the untagged version of 2MS2mut, the distribution of NLS-tagged protein was shifted towards the nucleus, but a significant amount remained in the

cytoplasm, such that the protein was present at approximately the same concentration in both compartments. Immunofluorescence microscopy of stable cell lines expressing the three localization variants of 2MS2mut using the same anti-MS2 antibody validated the subcellular distribution determined by immunoblotting (Figure 3.8B).

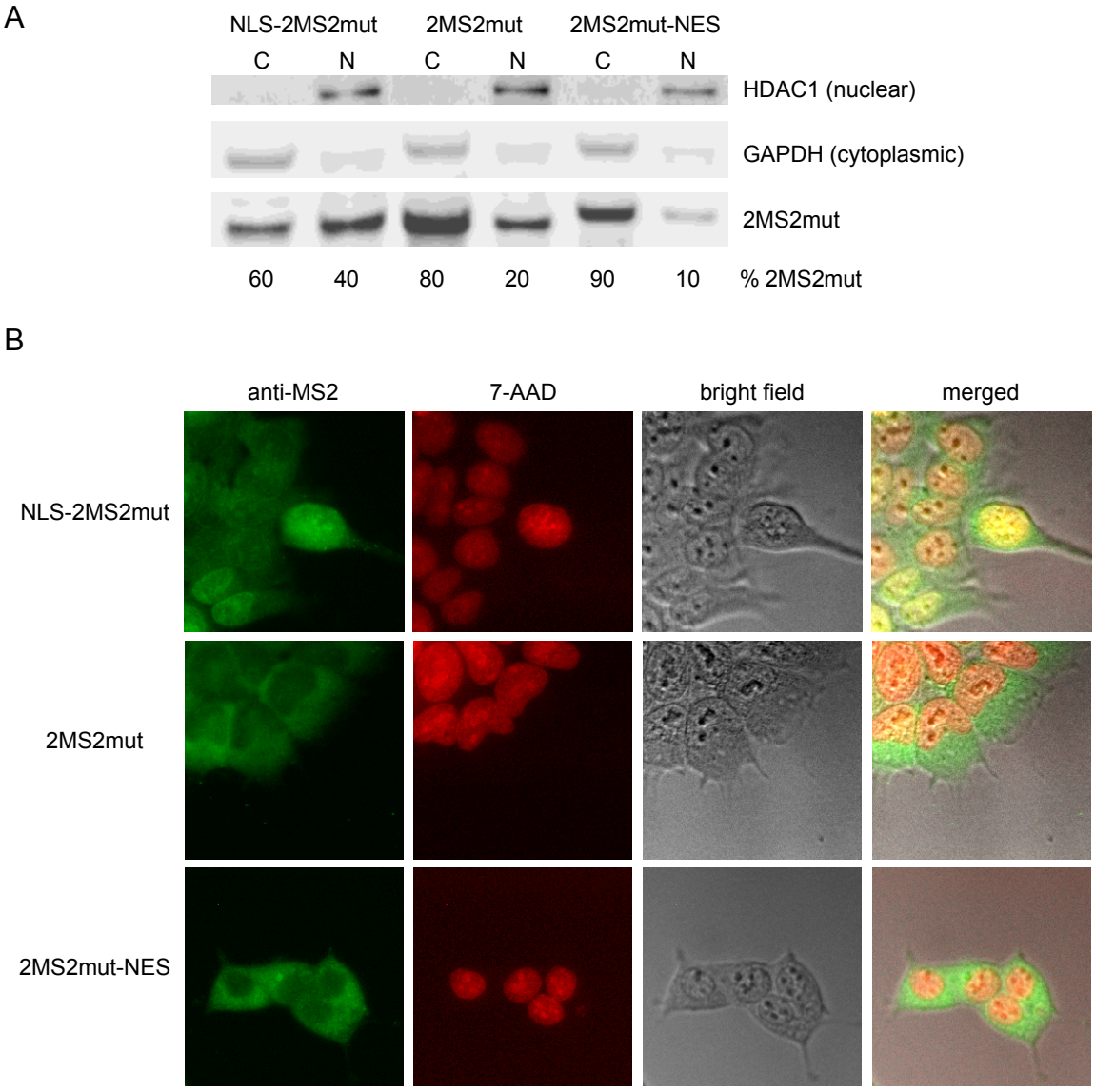

Figure 3.8. Subcellular localization of ligands with and without localization signals. (**A**) Immunoblot showing subcellular compartment distribution of 2MS2mut, NLS-2MS2mut,

and 2MS2mut-NES, along with nuclear and cytoplasmic controls. Percentages are calculated by normalizing quantified band intensity to the number of cells harvested. C, cytoplasm; N, nucleus; HDAC1, histone deacetylase 1; GAPDH, glyceraldehyde 3-phosphate dehydrogenase. (**B**) Immunofluorescence microscopy of 2MS2mut, NLS-2MS2mut, and 2MS2mut-NES using the same anti-MS2 antibody as in **A**. Green, anti-MS2 antibody and fluorescent secondary antibody; red, 7-aminoactinomycin D (7-AAD) nuclear stain.

We tested the localization-tagged versions of 2MS2mut with a subset of ribozyme switches in both transient and stable expression assays (Figure 3.9). While the switches responded similarly to 2MS2mut and 2MS2mut-NES, we observed that NLS-2MS2mut produced a slightly lower level of switching activity. As we have repeatedly observed by flow cytometry and immunoblotting that proteins with NLS tags are present at lower levels than untagged versions, we inferred that the lower switching activity was likely due to lower protein levels and not an effect of the altered subcellular distribution of the protein. Importantly, because the switches respond to 2MS2mut-NES, we concluded that cytoplasmic localization of the protein ligand is sufficient for switching activity, yielding as much as 5.3-fold ON switching with MS2-B11 and 4.3-fold OFF switching with MS2-C1 in a stable expression assay.

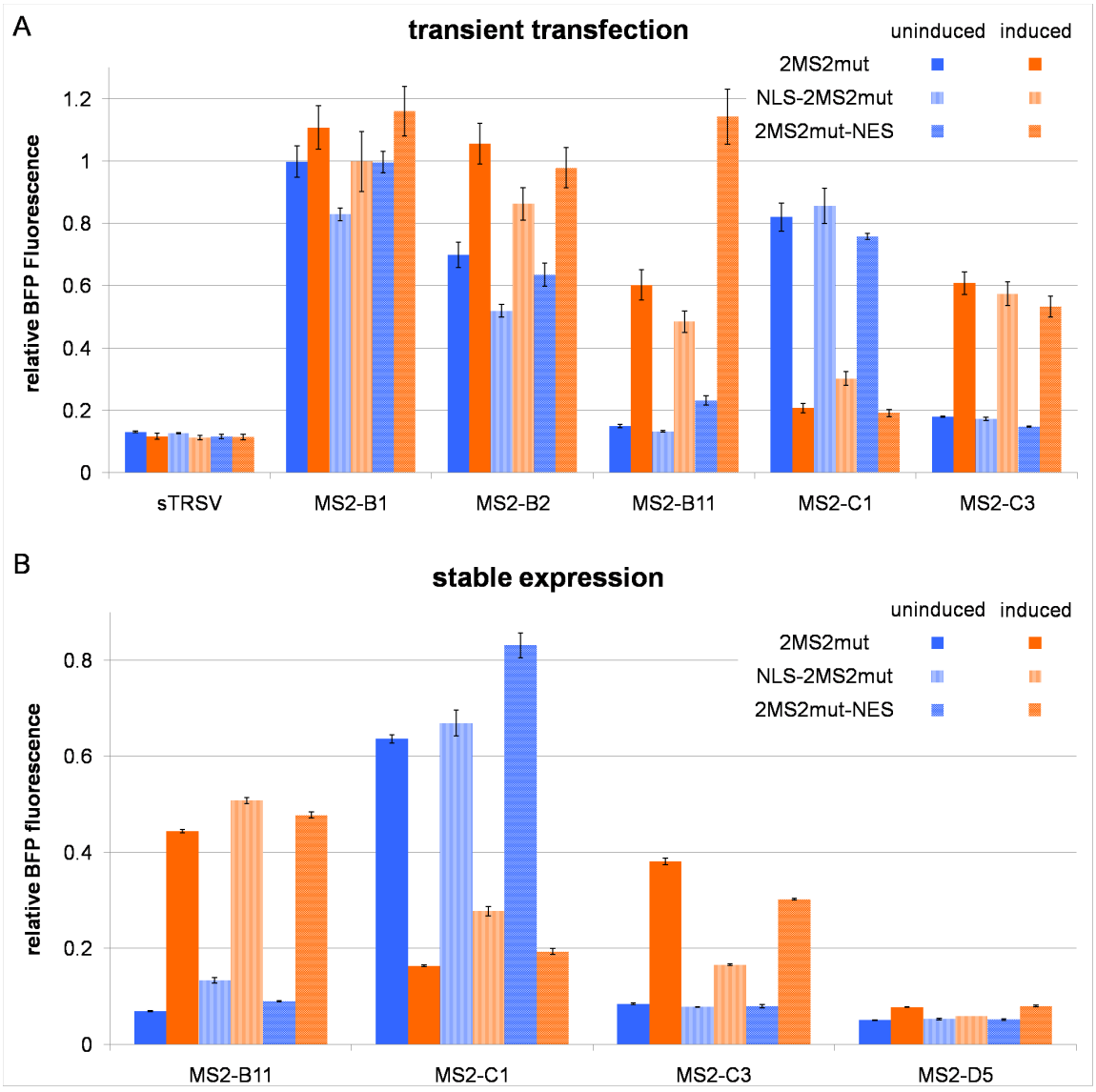

Figure 3.9. Activity of ribozyme switches with ligands with and without localization signals: 2MS2mut, NLS-2MS2mut, and 2MS2mut-NES. (**A**) Relative BFP fluorescence levels are reported for transiently transfected constructs encoding ribozyme switch sequences cotransfected with a transfection control plasmid. Reported values are geometric mean ± s.d. from biological duplicates and normalized to the non-cleaving sTRSVctrl. (**B**) Relative BFP fluorescence levels are reported for stably integrated constructs encoding ribozyme switch sequences. Reported values are geometric mean ±

s.d. from biological duplicates or triplicates and normalized to the non-cleaving sTRSVctrl.

As our NLS-2MS2mut protein failed to fully localize to the nucleus, we created new constructs to achieve the desired localization. We hypothesized that although NLS2-2MS2mut was being actively transported into the nucleus, its small size allowed it to passively diffuse out of the nucleus and accumulate in the cytoplasm to a significant level despite the NLS. We created 2MS2mut-DsRed fusion proteins with either an N-terminal NLS (NLS-2MS2mut-DsRed) or a C-terminal NES (2MS2mut-DsRed-NES), as well as 2MS2mut-DsRed without a localization sequence. These larger fusion proteins were expected to passively diffuse through the nuclear pore to a much lower extent than 2MS2mut without DsRed, and the fluorescent tag allowed for direct MS2 detection without immunostaining. We transiently transfected Flp-In T-REx HEK293 cells with plasmids encoding each of these three protein variants, induced MS2 expression from the CMV-TetO_2 promoter using doxycycline, and imaged the cells using confocal fluorescence microscopy (Figure 3.10). All three variants of the protein localized to the expected cellular locations. The presence in these constructs of BFP, which does not contain a localization signal and was found in both the nucleus and the cytoplasm, allowed for direct comparison between this protein and DsRed. While 2MS2mut-DsRed exhibited the same distribution throughout the cell as BFP, NLS-2MS2mut-DsRed was localized to the nucleus and 2MS2mut-DsRed-NES was localized to the cytoplasm.

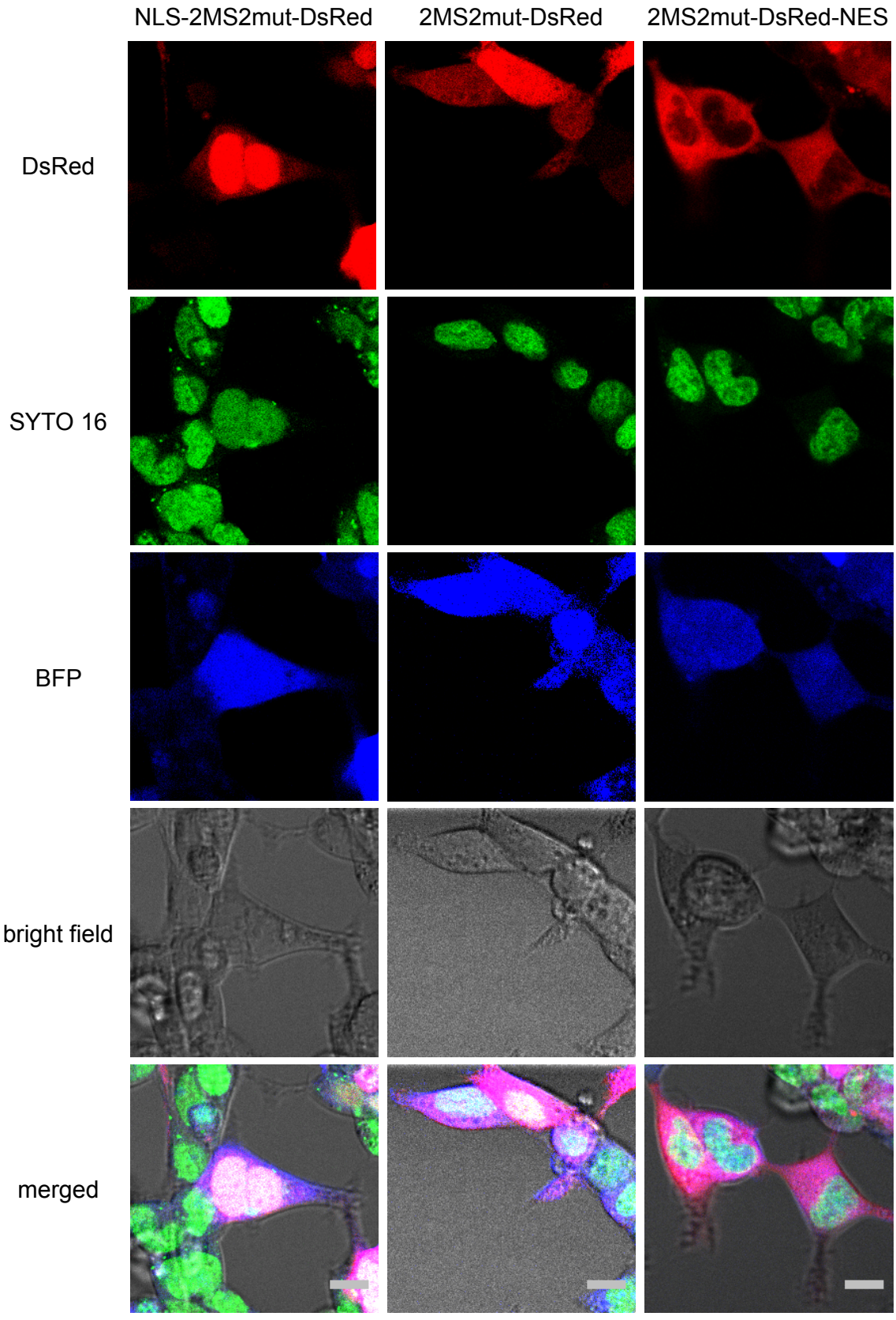
NLS-2MS2mut-DsRed
2MS2mut-DsRed
2MS2mut-DsRed-NES
DsRed
SYTO 16
BFP
bright field
merged

Figure 3.10. Confocal fluorescence microscopy of ligands with and without localization signals: 2MS2mut-DsRed, NLS-2MS2mut-DsRed, 2MS2mut-NES-DsRed. Red, DsRed; blue, BFP; green, SYTO 16 nuclear stain. Scale bars are 10 μm.

We tested the three 2MS2mut-DsRed variants with the best ON (MS2-B11) and OFF (MS2-C1) switch in a stable expression assay. As with 2MS2mut without DsRed, the switches responded to the nuclear-localized ligand to a lesser extent than to either the unlocalized or cytoplasmic-localized ligand, which yielded similar levels of response (MS2-B11: 3.6-fold for NLS, 6.4-fold for unlocalized, 6.5-fold for NES; MS2-C1: 2.8-fold for NLS, 4.6-fold for unlocalized, 4.3-fold for NES) (Figure 3.11). As described above, we assumed that the lower level of switch responsiveness to NLS-2MS2mut-DsRed was likely due to lower steady-state level of protein rather than a specific effect of nuclear localization of ligand.

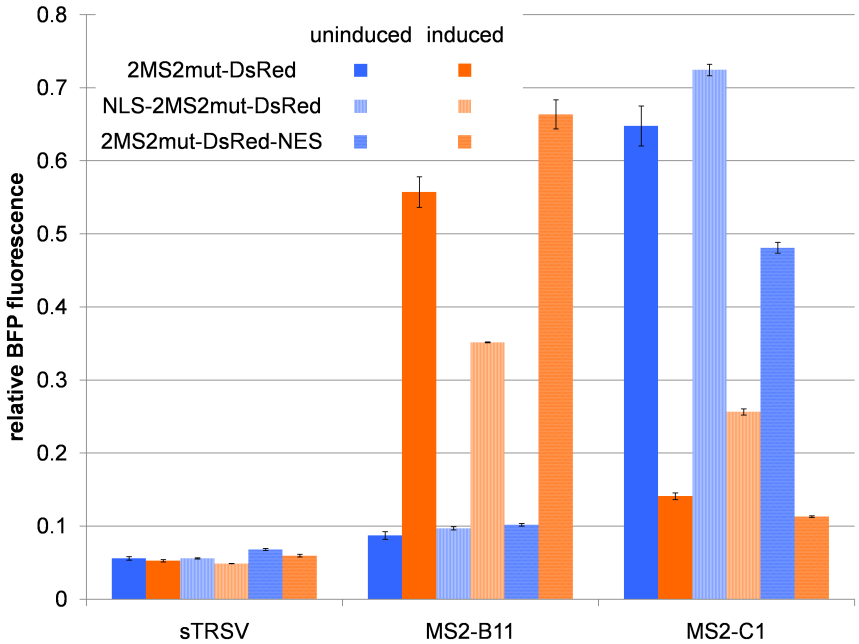

Figure 3.11. Activity of ribozyme switches with improved localized ligands: 2MS2mut-DsRed, NLS-2MS2mut-DsRed, and 2MS2mut-DsRed-NES. Relative BFP fluorescence levels are reported for stably integrated constructs encoding ribozyme switch sequences. Reported values are geometric mean ± s.d. from biological duplicates and normalized to the non-cleaving sTRSVctrl.

To examine the relationship between ligand expression level and switch response for the three localization variants of 2MS2mut-DsRed, we measured BFP regulation activity over a range of ligand inducer concentrations in a stable expression assay (Figure 3.12A). MS2-B11 and MS2-C1 exhibited a lower response to NLS-2MS2mut-DsRed than the other two ligand variants at all doxycycline concentrations tested. However, comparing BFP regulation activity to DsRed fluorescence (Figure 3.12B) reveals that all three protein variants yield similar switch activity at a given level of DsRed fluorescence. From these results we concluded that switch response is dependent on ligand expression level and not on its localization, and that nuclear and cytoplasmic localization of ligand are each sufficient for switching activity.

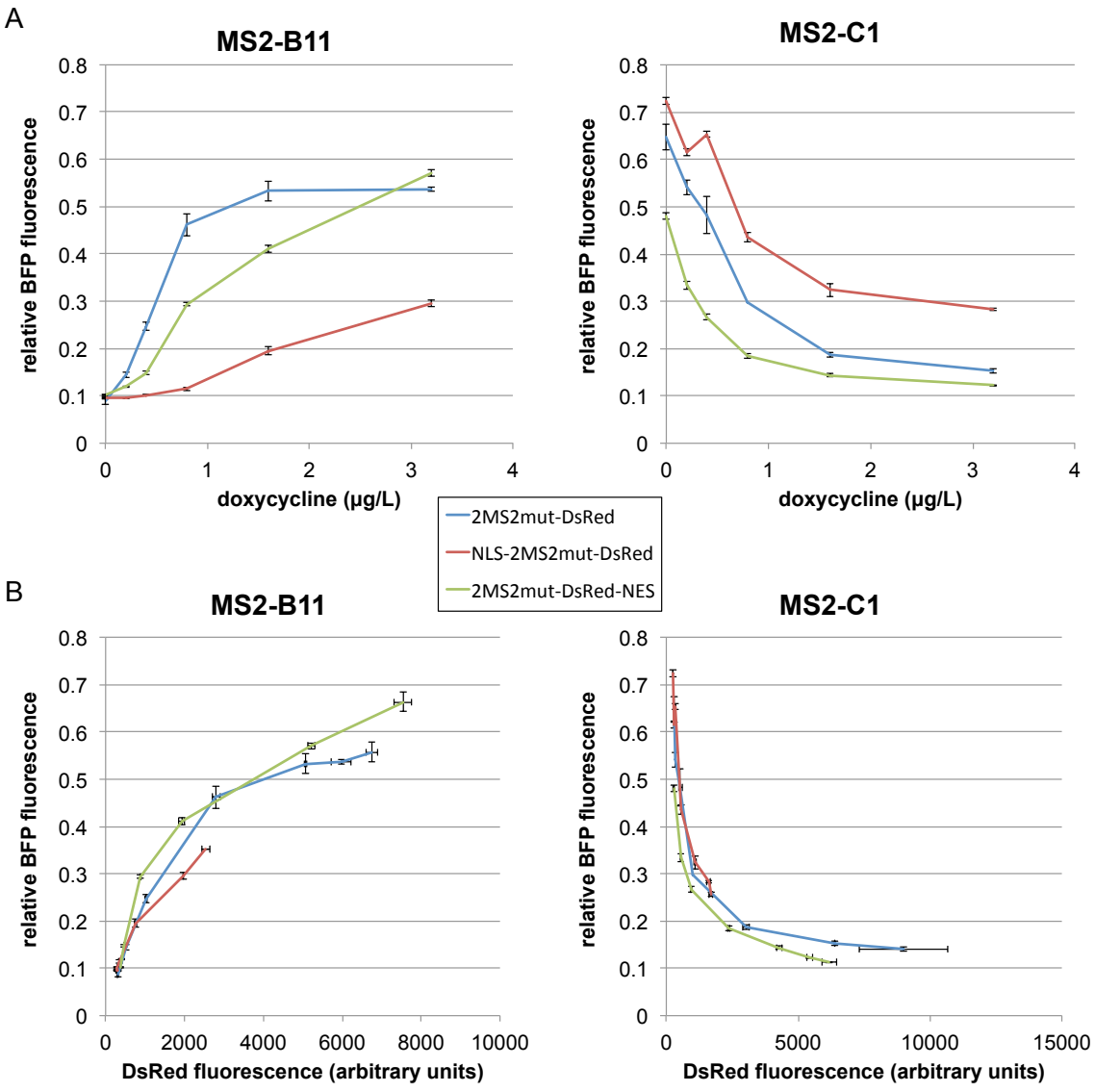

Figure 3.12. Activity of ribozyme switches with improved localized ligands over a range of ligand concentrations. (**A**) Reporter gene expression as a function of doxycycline concentration. Relative BFP fluorescence levels are reported for stably integrated constructs encoding ribozyme switch sequences. Reported values are geometric mean ± s.d. from biological duplicates and normalized to the non-cleaving sTRSVctrl. (**B**) Reporter gene expression as a function of DsRed fluorescence. The same data sets in B are plotted against DsRed fluorescence levels. Relative BFP and DsRed fluorescence

levels are reported for stably integrated constructs encoding ribozyme switch sequences. Reported values are geometric mean ± s.d. from biological duplicates and BFP values are normalized to the non-cleaving sTRSVctrl.

Development of ribozyme switch platforms responsive to additional proteins

We attempted to demonstrate the flexibility of our ribozyme switch platform by creating devices responsive to additional proteins. We chose two other bacteriophage proteins with demonstrated sequence-specific RNA binding, *Pseudomonas* phage PP7 coat protein[32] and the 1–22 peptide of lambda N protein[22,33]. We also chose nuclear factor κB (NF-κB) and β-catenin, two endogenous proteins involved in transcription and deregulated in many forms of cancer[7,34–38]. Aptamers to each of these proteins have been selected using SELEX and validated for *in vivo* function[39–42].

We designed three ribozyme switches containing the PP7 aptamer (Figure 3.13A). They are based on MS2-C3, which showed a high level of response to MS2, with the PP7 aptamer replacing the MS2 aptamer. The three designs differ from each other in the length of the aptamer stem beyond bulge II. Experiments were performed with transient expression assays using the improved characterization system (Figure 3.2), with the protein ligand expressed from the CMV-TetO_2 promoter. We used a mutant version of PP7 containing amino acid substitutions C68A and C71A to reduce multimerization while maintaining RNA binding affinity[43], similar to our strategy with the MS2 ligand. The data demonstrate little gene knockdown and no switching activity for any of the PP7 designs (Figure 3.13B).

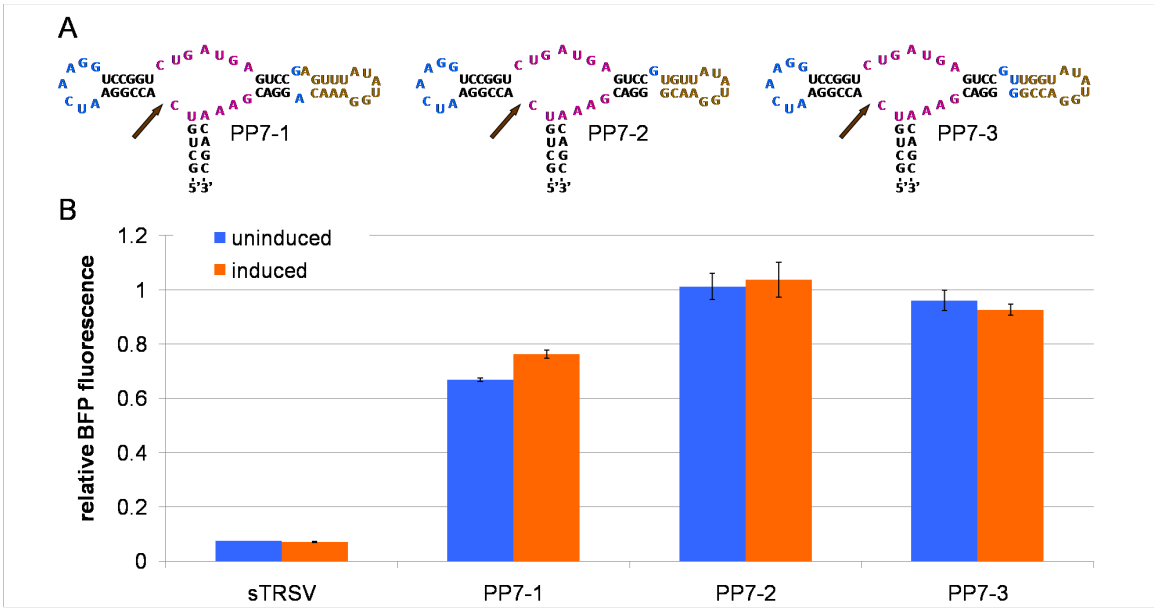

Figure 3.13. Design and testing of PP7-responsive switch designs. (**A**) Structures of the three designs. Coloring is the same as in Figure 3.1. (**B**) Activity of PP7-responsive switch designs. Relative BFP fluorescence levels are reported for transiently transfected constructs encoding ribozyme switch sequences cotransfected with a transfection control plasmid. Reported values are geometric mean ± s.d. from biological duplicates and normalized to the non-cleaving sTRSVctrl.

We designed four ribozyme switches containing the lambda N aptamer (Figure 3.14A). Lambda-1 is based on the previously characterized theophylline-responsive L2b8[11] and Lambda-2 is based on MS2-B11, with the lambda N aptamer replacing the theophylline and MS2 aptamers, respectively. The other two designs do not contain a transmitter component, and loop II is replaced by the lambda N aptamer loop in a similar fashion as the MS2-C designs (Figure 3.1). Experiments were performed with transient expression assays using the improved characterization system (Figure 3.2), with the protein ligand expressed from the CMV-TetO$_2$ promoter. The data demonstrate that the

four ribozyme switch designs exhibit a range of gene knockdown activity; however, none respond to lambda N (Figure 3.14B).

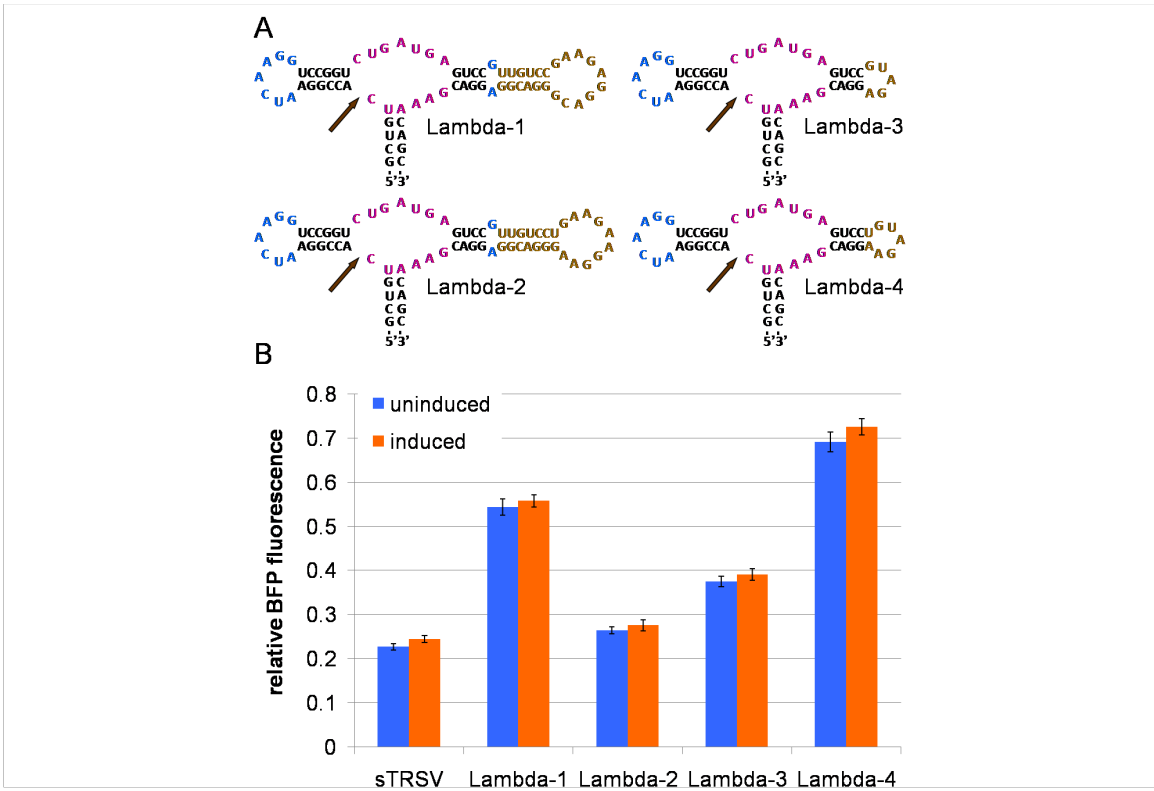

Figure 3.14. Design and testing of lambda-N-responsive switch designs. (**A**) Structures of the four designs. Coloring is the same as in Figure 3.1. (**B**) Activity of lambda-N-responsive switch designs. Relative BFP fluorescence levels are reported for transiently transfected constructs encoding ribozyme switch sequences. Reported values are geometric mean ± s.d. from biological duplicates and normalized to the non-cleaving sTRSVctrl.

We designed thirteen ribozyme switches containing the aptamer for the p50 subunit of NF-κB and five ribozyme switches containing the aptamer for the p65 subunit

(Figure 3.16A). These designs all contain transmitter components, similar to the MS2-B designs (Figure 3.1), differing from each other in the sequence identity of loop I and the transmitter. For each ligand we designed both ON and OFF switches.

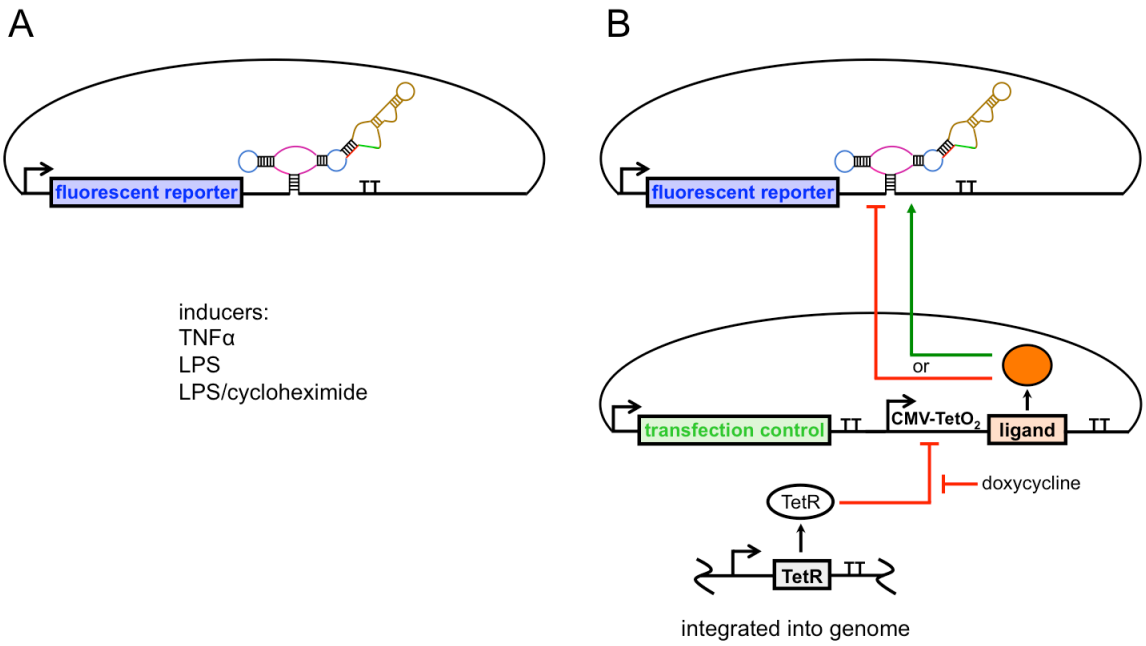

Figure 3.15. NF-κB-responsive ribozyme switch characterization system. (**A**) A fluorescent reporter (BFP) with ribozyme switch is encoded on a plasmid, which is transfected into a Flp-In T-REx HEK293 cell line. The NF-κB signaling pathway is induced with the addition of TNFα, LPS, or LPS in combination with cycloheximide. (**B**) The switch plasmid is cotransfected with a plasmid encoding the protein ligand (under the control of CMV-$TetO_2$) and a fluorescent transfection marker. Addition of doxycycline derepresses the CMV-$TetO_2$ promoter, turning on expression of the ligand, which regulates the activity of ON and OFF switches. Cotransfections were also performed in conjunction with LPS induction.

We employed several different strategies in attempting to elicit switch response to NF-κB ligand. The NF-κB p50/p65 heterodimer is normally bound to the inhibitor IκB, which blocks its NLS, preventing import into the nucleus[44]. Upon activation of the NF-κB pathway, IκB is targeted for ubiquitin-dependent degradation, releasing NF-κB to translocate into the nucleus and activate transcription of its target genes[34]. It is expected that NF-κB will not bind to its aptamer when inhibited, as IκB stabilizes NF-κB in a conformation with very weak nucleic acid affinity[45–47]. After transfecting Flp-In T-REx HEK293 cells with plasmids encoding our switches, we activated the NF-κB pathway with tumor necrosis factor α (TNFα), lipopolysaccharide (LPS), or LPS in combination with cycloheximide (Figure 3.15). We also tried expressing p50 and p65 heterologously, in cotransfections of a plasmid encoding the protein and a plasmid encoding a cognate switch. Finally, we tried heterologous protein expression in combination with LPS induction. Although the designs exhibited a range of gene knockdown activity, none of them displayed switching activity under any of the conditions tested (Figure 3.16B).

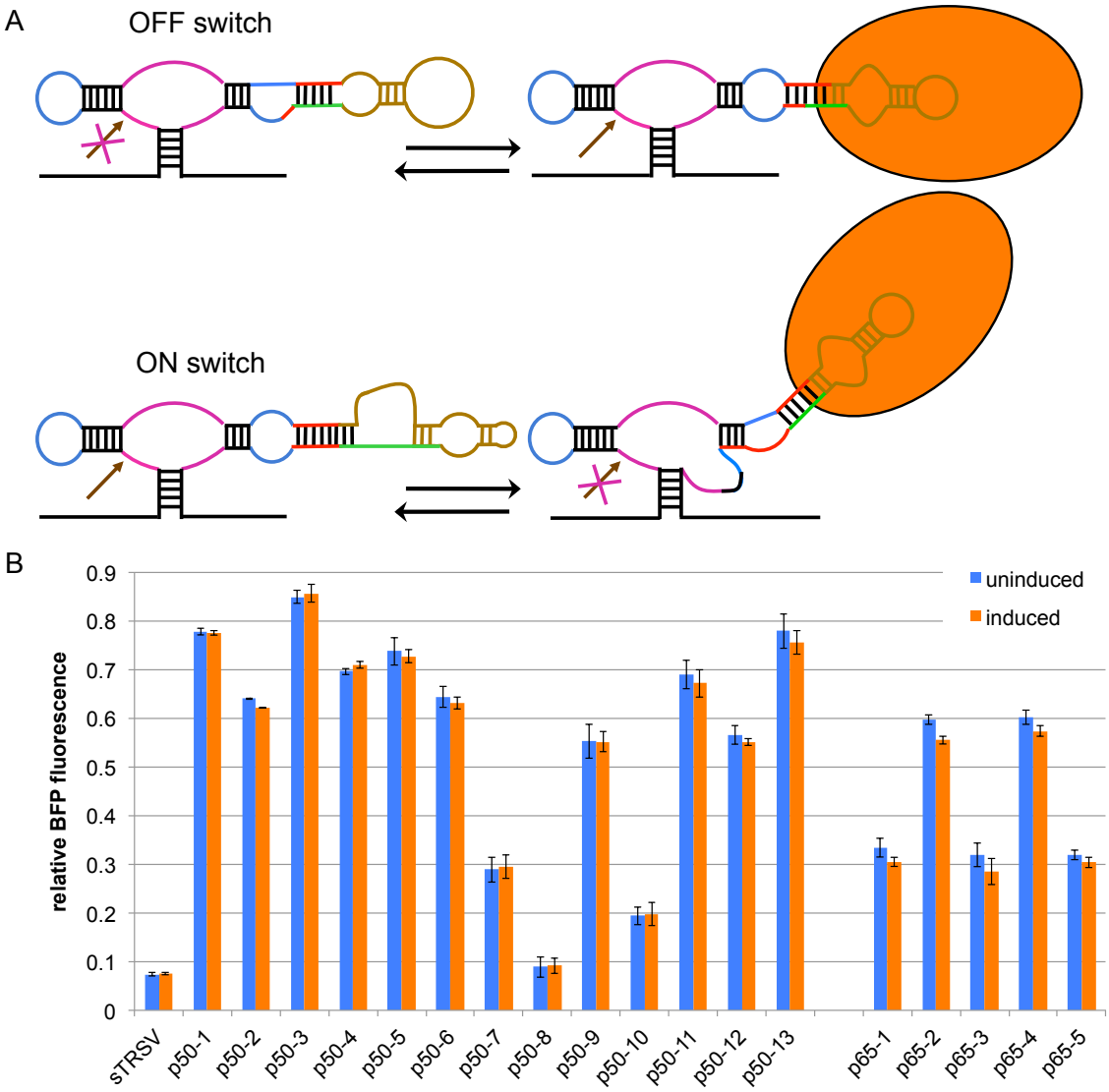

Figure 3.16. Design and testing of NF-κB-responsive switch designs. (**A**) ON and OFF switches were designed with aptamers for p50 and p65 subunits of NF-κB. Coloring is the same as in Figure 3.1. See Supplementary Table 3.1 for sequences. (**B**) Activity of NF-κB-responsive switch designs. Relative BFP fluorescence levels are reported for transiently transfected constructs encoding ribozyme switch sequences cotransfected with a plasmid encoding p50 or p65 and a fluorescent transfection control. Reported values

are geometric mean ± s.d. from biological duplicates and normalized to the non-cleaving sTRSVctrl.

We designed two sets of ribozyme switches containing the β-catenin aptamer (Figure 3.17A). In one set of designs (Bcat-A) the β-catenin aptamer replaced loop I of four different hammerhead ribozymes similar in sequence and structure to sTRSV (sLTSV−, sLTSV+, CChMVd−, and SCMoV+), following a similar strategy as the MS2-C designs. The other set of designs (Bcat-B) was similar to the MS2-responsive sequential aptamer and ribozyme designs (MS2-D), with the β-catenin aptamer just upstream of the ribozyme. These six designs varied in the length and sequence identity of the transmitter component.

A

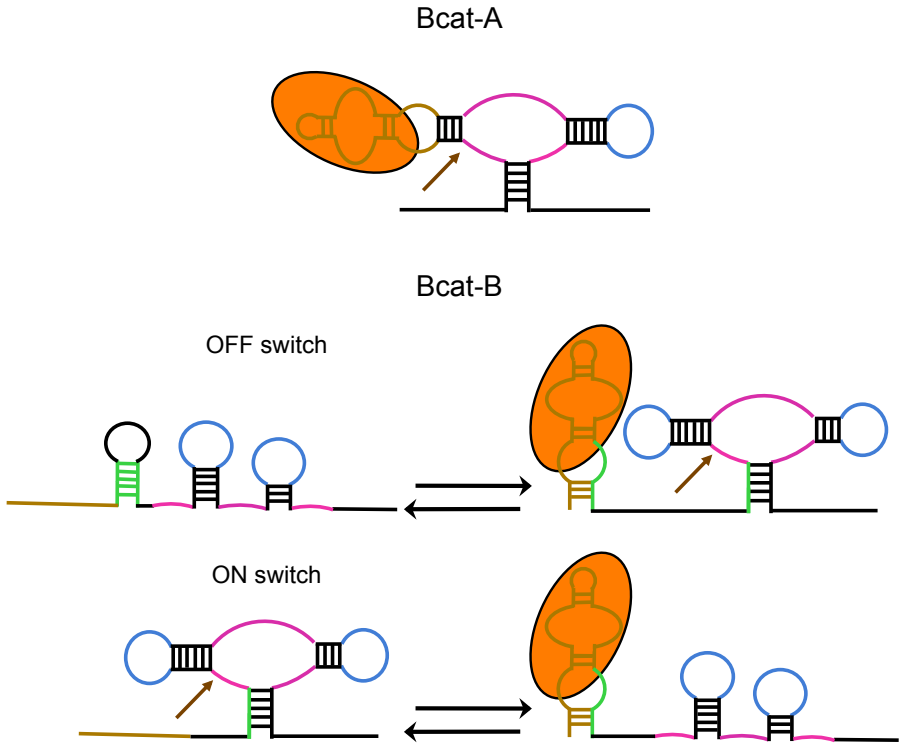
Bcat-A
Bcat-B
OFF switch
ON switch

B

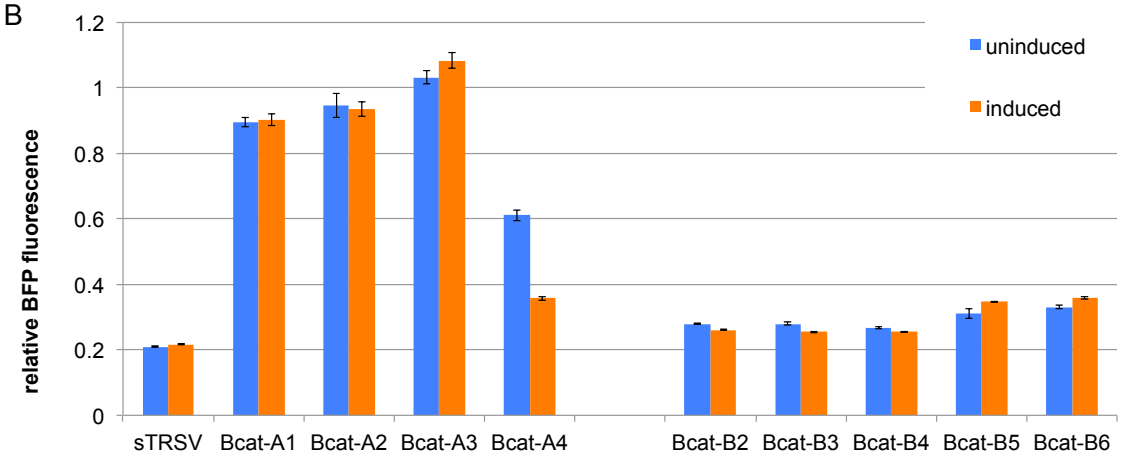
relative BFP fluorescence
1.2
1
0.8
0.6
0.4
0.2
0
uninduced
induced
sTRSV
Bcat-A1
Bcat-A2
Bcat-A3
Bcat-A4
Bcat-B2
Bcat-B3
Bcat-B4
Bcat-B5
Bcat-B6

C

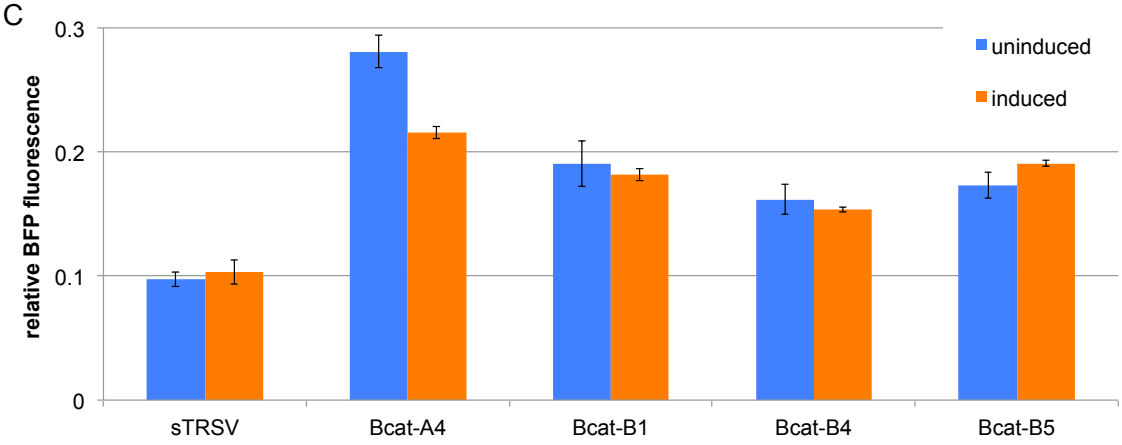
relative BFP fluorescence
0.3
0.2
0.1
0
uninduced
induced
sTRSV
Bcat-A4
Bcat-B1
Bcat-B4
Bcat-B5

Figure 3.17. Design and testing of β-catenin-responsive switch designs. (**A**) β-catenin-responsive loop I replacement (Bcat-A) and sequential aptamer and ribozyme (Bcat-B) switch designs. Coloring is the same as in Figure 3.1. See Supplementary Table 3.1 for sequences. (**B**) Activity of β-catenin-responsive switch designs in a transient expression assay. Relative BFP fluorescence levels are reported for transiently transfected constructs encoding ribozyme switch sequences. Reported values are geometric mean ± s.d. from biological duplicates and normalized to the non-cleaving sTRSVctrl. (**C**) Activity of β-catenin-responsive switch designs in a transient expression assay with transfection control. Relative BFP fluorescence levels are reported for transiently transfected constructs encoding ribozyme switch sequences cotransfected with a transfection control plasmid. Reported values are geometric mean ± s.d. from biological duplicates and normalized to the non-cleaving sTRSVctrl.

β-catenin translocates into the nucleus upon activation of the Wnt signaling pathway, and in the absence of signaling is phosphorylated and degraded by the proteasome[38]. After transfecting Flp-In T-REx HEK293 cells with plasmids encoding our switches, we activated the pathway with the addition of the cytokine Wnt3A to the cell culture media but observed no switch response. We also tried heterologously expressing the Arm 1–12 domain of β-catenin[48], which has been shown to have higher affinity for the aptamer than the full-length protein[49], from the CMV-TetO_2 promoter in a transient transfection assay, as we did with the MS2 proteins (Figure 3.2). Most of the loop I replacement designs (Bcat-A) exhibited little gene knockdown activity, while the sequential designs (Bcat-B) exhibited high levels of gene knockdown activity, similar to

the MS2-D designs (Figure 3.17B). Only one design, Bcat-A4, exhibited responsiveness to heterologous β-catenin in this experimental system. Induction with Wnt3A in addition to the heterologous expression of β-catenin had no effect on switch activity. We reexamined four switch designs in an assay with a transfection control plasmid and Bcat-A4 exhibited 1.3-fold OFF-switching (Figure 3.17C). Stable integration of the Bcat-A4 and heterologous β-catenin construct into Flp-In T-REx HEK293 cells resulted in no switch response, likely due to the ligand being expressed at a lower level than in transient transfections, as described above (Figure 3.5).

Discussion

We developed protein-responsive gene-regulatory devices based on the ribozyme switch platform previously developed in the Smolke laboratory[11]. We first screened a large number of designs with different architectures, and found that directed conformational changes of ribozyme structure are important for ligand responsiveness. Specifically, coupling the MS2 aptamer directly to a ribozyme loop, without a transmitter component (MS2-A), resulted in devices that did not respond to MS2 ligand. Designs containing a transmitter that altered the structure of the stem and catalytic core (MS2-B), analogous to previously developed ribozyme switches[11], were among the most highly functional switch designs tested. The designs containing a transmitter that altered the structure of the stem and loop (MS2-C) also led to functional switches. Three transmitter designs, MS2-B1, MS2-B3, and MS2-B7, were altered by replacing loop I with an alternative sequence, generating MS2-B2, MS2-B10, and MS2-B11. In all three cases

the altered loop resulted in improved gene knockdown and switching activity (Figure 3.7B). The sequential designs, with the aptamer immediately upstream of the ribozyme in the transcript (MS2-D), were mostly insensitive to ligand but one (MS2-D5) exhibited a moderate amount of switching activity (up to 2.4-fold) and the lowest basal expression level of all designs tested, with gene knockdown activity comparable to wild-type ribozyme (sTRSV).

We further improved our characterization system by optimizing the MS2 ligand. Responsiveness to wild-type MS2 in our initial switch characterization study was at most 1.8-fold (Figure 3.4, MS2-B2). Replacing wild-type MS2 with a mutant containing two amino acid substitutions that prevent multimerization[27] improved sensitivity for most of the switches tested (Figure 3.7A). The fused dimer of this mutant MS2 elicited an even greater switch response, including from MS2-B1, which was unresponsive to the wild-type and mutant monomer (Figure 3.7A). We concluded that the fused dimer of mutant MS2 was the best ligand for characterizing our switch designs.

Using our optimized ligand we were able to demonstrate high levels of ON-switching with MS2-B11 (up to 4.1-fold) and OFF-switching with MS2-C1 (up to 3.8-fold). In contrast, previously described small-molecule-responsive ribozyme switches from the Smolke laboratory[15,17] have exhibited at most 2.1-fold ON switching (L2b18tc, tetracycline-responsive) and 1.7-fold OFF-switching (Lb2OFF, theophylline-responsive) in human cell lines. Switching activity was improved by incorporating multiple copies of the ribozyme switch into the 3' UTR of the target gene, resulting in up to 3.5-fold ON-switching (L2b8, 2 copies and L2b9, 3 copies)[17]. However, OFF switch activity has not been improved by this method.

We demonstrated the localization requirements of our ribozyme switches by assaying for sensitivity to our optimized ligand with fused localization signals. The initial implementation of these localization signals did not fully direct the protein to the desired subcellular compartment (Figure 3.8). Although the NES-tagged protein was present in the nucleus at levels no higher than a cytoplasmic control protein, the NLS-tagged protein was present in both the nucleus and the cytoplasm. We hypothesized that despite the fusion with localization signals the protein was passively diffusing through the nuclear pore due to its small size. We therefore created fusion proteins with DsRed, whose increased size was predicted to prevent passive diffusion through the nuclear pore and result in full localization, which was verified with confocal fluorescence microscopy (Figure 3.10).

Testing of localized variants of 2MS2mut-DsRed with MS2-B11 and MS2-C1 revealed little dependence of switch activity on ligand localization. Unlocalized and cytoplasmic-localized ligands elicited similar levels of response for each switch, while the nuclear-localized ligand elicited much lower levels of response (Figure 3.11). We have observed by flow cytometry that NLS-tagged fluorescent proteins generate fluorescence levels less than half those of analogous untagged proteins (Figure 3.12B and Ryan Bloom, unpublished results). It is possible that the addition of the seven-amino-acid NLS to the N-terminus of a fluorescent protein affects its three-dimensional structure in a way that negatively impacts its fluorescent output; however, we believe this is unlikely. Immunoblotting indicates that the total amount of MS2 protein per cell is lower with the NLS tag than without (Figure 3.8A), suggesting that the lower level of fluorescence observed from NLS-tagged proteins is due to lower steady-state protein

levels and not to a decrease in fluorescence output per molecule. This conclusion is further supported by our finding that switch response is dependent on ligand expression level as measured by fluorescence (Figure 3.12B). Assuming that each of the three localization variants of 2MS2mut-DsRed exhibits roughly the same fluorescence output per molecule, the data show that switch response is correlated with ligand expression level regardless of localization.

Nuclear and cytoplasmic localization of ligand each appear to be sufficient for switching activity in human cells. This is somewhat surprising for an ON switch such as MS2-B11, which cleaves in the absence of ligand. One might expect this switch to cleave during or immediately after transcription if ligand is absent from the nucleus, or to cleave after nuclear export if ligand is absent from the cytoplasm. However, our data did not support these initial expectations.

Although our confocal fluorescence microscopy measurements show clear localization, we cannot rule out the possibility that a small amount of the NLS-tagged ligand is found in the cytoplasm and a small amount of the NES-tagged ligand is found in the nucleus. The presence of such mislocalized protein could prevent precise examination of the effect of ligand localization on ribozyme switch activity if that small amount were sufficient to prevent ribozyme ON switch cleavage. However, the correlation between switch response and DsRed fluorescence (Figure 3.12B) suggests that this is unlikely. If, for example, nuclear localization were necessary for switch activity, and switches appeared to respond to NES-tagged ligand, we would expect the required amount of NES-tagged ligand expression to be much higher than NLS-tagged ligand to yield the same level of switch activity, as most of the NES-tagged protein would

be in the cytoplasm and unable to affect the switch. We observed that similar ligand expression levels, as measured by fluorescence, resulted in similar levels of switching regardless of localization signal.

Our data suggest that the ribozyme switches do not cleave before nuclear export to a significant degree, nor do they cleave in the cytoplasm to a significant degree when the ligand is present in the nucleus. We speculate that ribozyme cleavage in the nucleus is low, possibly due to prevention of proper folding by binding of proteins that form the messenger ribonucleoprotein (mRNP). This would minimize ribozyme cleavage before the switch is exposed to cytoplasmic-localized ligand. When ligand is localized to the nucleus, we speculate that it is able to bind to the aptamer and is carried out of the nucleus by the mRNA during nuclear export. The ability of mRNA containing an aptamer to carry MS2 out of the nucleus has been previously demonstrated[20], but this behavior may depend on the small size of the MS2 protein and not be generalizable to larger proteins. After export to the cytoplasm, dissociation of the ligand from the ribozyme switch would be favored due to the extremely low local concentration of free ligand. A low ligand off-rate and a low ribozyme cleavage rate would both contribute to allowing the mRNA to be translated before cleavage. Functional MS2-responsive ribozyme switches presented here exhibit off rate constants in the range of 0.001–0.05 s^{-1} (Andrew Kennedy, unpublished results) and cleavage rate constants in the range of 0.05–1 min^{-1} (Andrew Kennedy, unpublished results). ON switches with higher cleavage rates would be expected to be less responsive to localized ligand (nuclear or cytoplasmic), and ON switches with higher ligand off-rates would be expected to be less responsive to nuclear-localized ligand.

In the future the ribozyme switch mechanism of action could be more thoroughly investigated. Studies using switches with a range of cleavage-rate constants and ligand off-rate constants would establish the relationship between these parameters and *in vivo* response to localized ligands. This in turn would confirm or disprove our supposition that nuclear and cytoplasmic localization are each sufficient for switching activity. If it is indeed true that ligand localization does not negatively impact switching activity, then our ribozyme switch platform would be capable of sensing proteins in the nucleus or the cytoplasm. In contrast, switches based on regulation of shRNA processing[9] or splicing[10] are limited to sensing cytoplasmic or nuclear proteins, respectively.

We attempted to develop ribozyme switches responsive to additional proteins. We suspected that generating switches with aptamers for bacteriophage proteins (PP7 and lambda N) would be straightforward, basing our designs on functional MS2-responsive switches. However, none of these designs responded to ligand. We next attempted to generate ribozyme switches responsive to NF-κB and β-catenin, two proteins involved in transcription and deregulated in many forms of cancer[7,34–37], for which there exist *in vitro* selected aptamers with validated *in vivo* function[39–42]. Although NF-κB and β-catenin are endogenously expressed in our human cell line, we did not expect them to be available for binding to ribozyme switches without activation of their signaling pathways or heterologous overexpression. We were unable to demonstrate NF-κB-responsiveness, but one β-catenin switch, Bcat-A4, exhibited 1.3-fold OFF-switching in response to transient heterologous expression of β-catenin. We suspect that Bcat-A4 did not respond to endogenous or stably expressed β-catenin because the steady-state levels of protein were too low. In the future high-throughput *in vivo* screening methods[50–52] could be used

to assay large libraries of devices to explore a wider design space and achieve greater success generating functional switches responsive to new protein ligands.

The protein-responsive ribozyme switch platform we have developed is unique in its ability to respond to ligands in both the nucleus and the cytoplasm, while previously reported protein-responsive switches can function in only one compartment[9,10,53,54]. One potential limitation of our platform is that it is not able to detect changes in protein localization. However, our platform's capability of sensing both nuclear and cytoplasmic proteins may be an important advantage for its use as a noninvasive reporter or phenotypic controller in future applications.

Methods

Plasmid construction

All plasmids were constructed using standard molecular biology techniques. Oligonucleotides were synthesized by Integrated DNA Technologies and the Stanford Protein and Nucleic Acid Facility. Cloning enzymes, including restriction enzymes and T4 DNA ligase, were obtained from New England Biolabs. Ligation products were electroporated into *Escherichia coli* DH10B (Life Technologies) using a GenePulser XP (Bio-Rad Laboratories) system or transformed into *E. coli* One Shot Top 10 (Life Technologies) using standard methods. Clones were screened using colony polymerase chain reaction (PCR) and verified by sequencing (Elim Biopharmaceuticals). 15% glycerol stocks were made from *E. coli* in logarithmic growth phase and stored at −80°C.

A standardized cloning method was developed to facilitate insertion of ligand-responsive devices and ligand coding regions into a single plasmid backbone. A DNA fragment encoding d2EGFP with a bGHpA signal and the CMV-TetO2 promoter was synthesized by GeneArt (Life Technologies) and inserted into pcDNA5/FRT (Life Technologies) between the restriction sites AflII/KpnI to form pCS2304 (Figure 3.18), which contained a CMV promoter expressing d2EGFP and FRT recombinase sites compatible with stable integration into the genome of Flp-In T-REx HEK293 cells (Life Technologies) to create isogenic stable cell lines. The coding region of the fusion protein MS2-DsRedMonomer was PCR amplified from pCS1392 (courtesy Stephanie Culler) using the primers No NLS A/X Fwd and DsRed A/X Rev and inserted into pCS2304 between XhoI/ApaI to form pCS2359. MS2-responsive ribozyme switch designs were inserted into pCS2359 between AvrII/AscI.

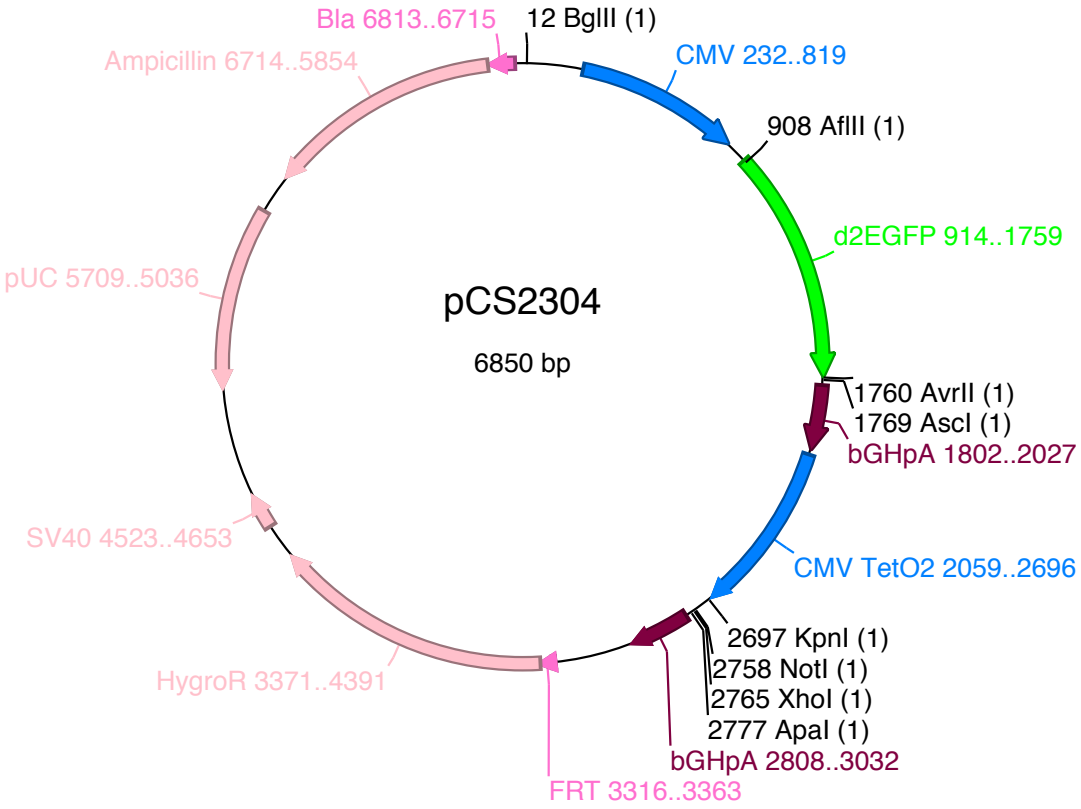
pCS2304
6850 bp
Bla 6813..6715
12 BglII (1)
Ampicillin 6714..5854
CMV 232..819
908 AflII (1)
d2EGFP 914..1759
pUC 5709..5036
1760 AvrII (1)
1769 AscI (1)
bGHpA 1802..2027
SV40 4523..4653
CMV TetO2 2059..2696
2697 KpnI (1)
2758 NotI (1)
2765 XhoI (1)
2777 ApaI (1)
HygroR 3371..4391
bGHpA 2808..3032
FRT 3316..3363

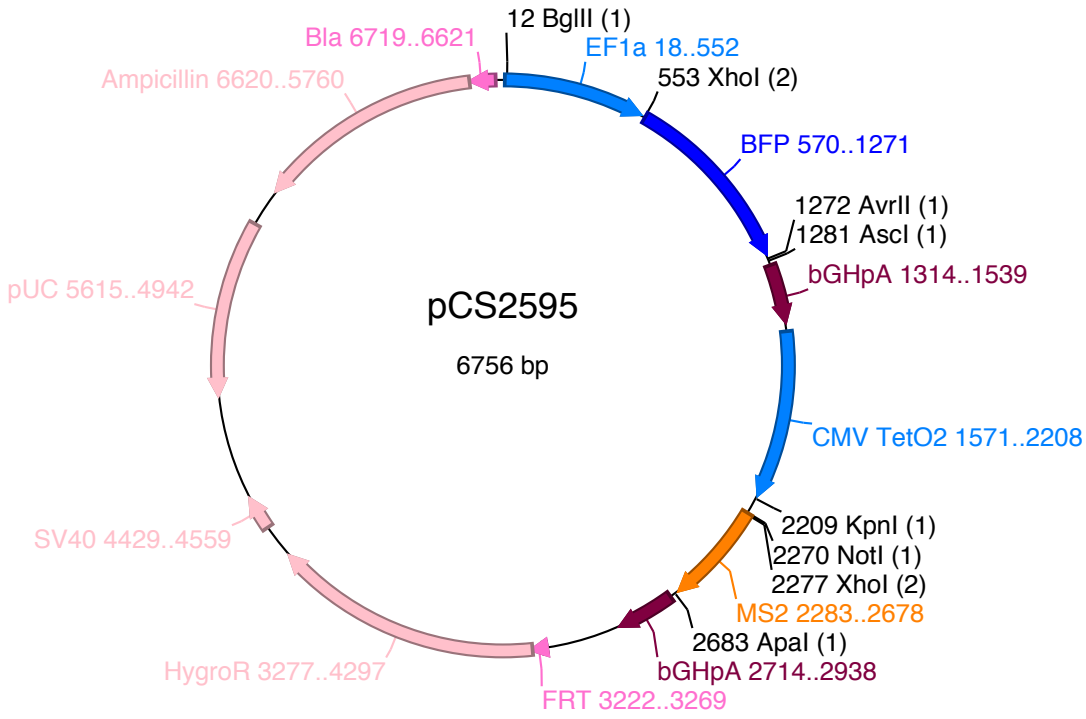
pCS2595
6756 bp
12 BglII (1)
Bla 6719..6621
EF1a 18..552
Ampicillin 6620..5760
553 XhoI (2)
BFP 570..1271
1272 AvrII (1)
1281 AscI (1)
pUC 5615..4942
bGHpA 1314..1539
CMV TetO2 1571..2208
2209 KpnI (1)
SV40 4429..4559
2270 NotI (1)
2277 XhoI (2)
MS2 2283..2678
2683 ApaI (1)
bGHpA 2714..2938
HygroR 3277..4297
FRT 3222..3269

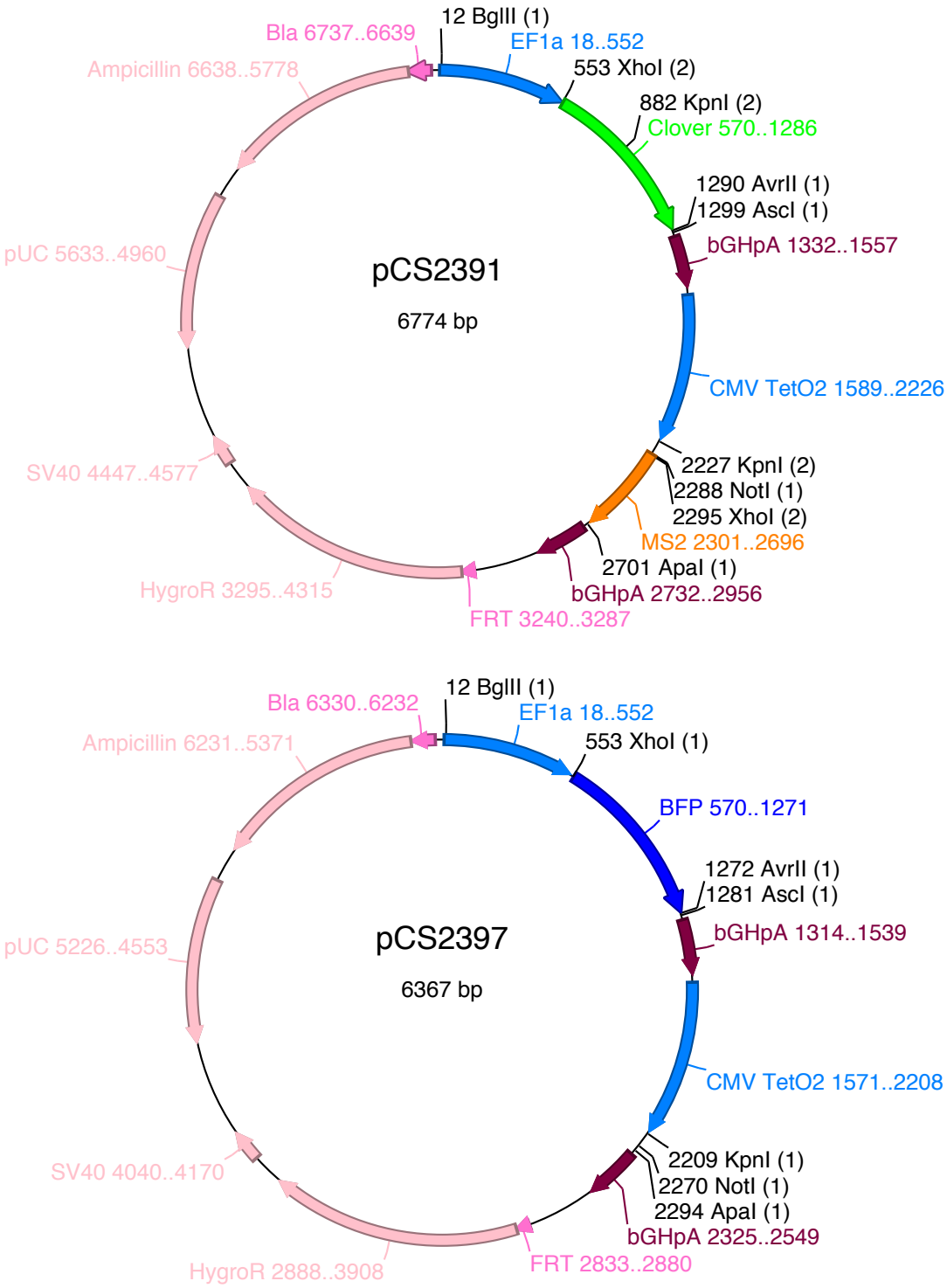

Figure 3.18. Plasmid maps.

An Ef1α promoter with the coding region of BFP was PCR amplified from pCS2585 (courtesy Melina Mathur) using the primers EF1BFP Fwd and EF1BFP Rev and inserted between BglII/AvrII, and the coding region of MS2 was PCR amplified from pCS1392 using No NLS A/X Fwd and MS2 A/X Rev and inserted between XhoI/ApaI into pCS2304 to form pCS2595 (Figure 3.18). MS2-responsive ribozyme switch designs were inserted into pCS2595 between AvrII/AscI.

The plasmid pCS2359 was digested with NheI/AvrII to remove d2EGFP and ligated to form pCS2406. The coding region of MS2 was PCR amplified from pCS1392 using the primers No NLS A/X Fwd and MS2 A/X Rev and inserted into pCS2406 between XhoI/ApaI to form pCS2409.

The coding region of MS2mut (V75E/A81G) was PCR amplified from the MBP-MS2-His plasmid (courtesy Rachel Green, Department of Molecular Biology and Genetics, Johns Hopkins University) using the primers MS2 NotI F and MS2 ApaI R and inserted into pCS2595 between NotI/ApaI to form pCS2631. MS2-responsive ribozyme switch designs were inserted into pCS2631 between AvrII/AscI.

A DNA fragment encoding 2MS2mut (MS2 V75E/A81G head-to-tail fused dimer) was synthesized by GeneArt (Life Technologies) and inserted into pCS2595 between NotI/ApaI to form pCS2686. The coding region of 2MS2mut was PCR amplified from pCS2686 using the primers NLS MS2 F and 2MS2mut R to add an N-terminal NLS, and using the primers 2MS2mut F and NES MS2 R to add a C-terminal NES, and inserted into pCS2595 between NotI/ApaI to form pCS2747 and pCS2787, respectively. MS2-responsive ribozyme switch designs were inserted into pCS2686, pCS2747, and pCS2787 between AvrII/AscI.

The coding region of DsRedMonomer was PCR amplified from pCS2359 using the primers DsRed GF and DsRed GR, and using the primers DsRed GF and DsRed NES R to add a C-terminal NES. The resulting DNA fragments were inserted into plasmids digested with ApaI using Gibson assembly[55] as follows: DsRed into pCS2686 to form pCS2897, DsRed into pCS2747 to form pCS2902, and DsRed-NES into pCS2686 to form pCS2907. MS2-responsive ribozyme switch designs were inserted into pCS2897, pCS2902, and pCS2907 between AvrII/AscI.

The coding region of Clover GFP was PCR amplified from pCS2586 (courtesy Melina Mathur) using the primers GF Clover and GR Clover, and pCS2595 was PCR amplified using the primers GF EF1 and GR EF1. The resulting DNA fragments were assembled using Gibson assembly[55] to form pCS2391 (Figure 3.18), which contained Clover GFP in place of BFP.

The coding region of the PP7 coat protein was PCR amplified from Addgene plasmid 28174 (Kathleen Collins) using the primers PP7 NotI F and PP7 ApaI R and inserted into pCS2595 between NotI/ApaI to form pCS2847. PP7-responsive ribozyme switch designs were inserted into pCS2847 between AvrII/AscI.

The DNA fragment lambda N was inserted into pCS2595 between NotI/ApaI to form pCS2816. Lambda-N-responsive ribozyme switch designs were inserted into pCS2816 between AvrII/AscI.

The DNA fragment insertNA was inserted into pCS2595 between NotI/ApaI to form pCS2397 (Figure 3.18). NF-κB-responsive ribozyme switch designs were inserted into pCS2397 between AvrII/AscI. The coding region of NF-κB p50 was PCR amplified from pCS1806 (courtesy Stephanie Culler) using the primers p50 NotI F and p50 ApaI R

and inserted into pCS2391 between NotI/ApaI to form pCS2604. The coding region of NF-κB p65 was PCR amplified from pJ1448 (courtesy Louis Maher III, Department of Biochemistry and Molecular Biology, Mayo Clinic College of Medicine) using the primers p65 NotI F and p65 ApaI R and inserted into pCS2391 between NotI/ApaI to form pCS2605.

β-catenin-responsive ribozyme switch designs were inserted into pCS2397 between AvrII/AscI. The coding region of β-catenin Arm 1–12 was PCR amplified from Addgene plasmid 17198 (Randall Moon) using the primers b-cat NotI F and b-cat ApaI R and inserted into pCS2595 between NotI/ApaI to form pCS2824. β-catenin-responsive ribozyme switch designs were inserted into pCS2824 between AvrII/AscI.

Human cell culture

Flp-In T-REx HEK293 cells (Life Technologies) were cultured in 10 mL (10 cm dish) or 3 mL (6 cm dish) Dulbecco's Modified Eagle's medium (DMEM) (Life Technologies) supplemented with 10% fetal bovine serum (FBS) (Life Technologies), 100 mg/L zeocin (Life Technologies), and 5 mg/L blasticidin (Life Technologies) in a humidified incubator at 37°C and 5% CO_2. Cells were seeded at $2x10^4$ cells/mL and passaged regularly using 0.25% trypsin-EDTA (Life Technologies), with media replaced every 48–72 hours. Cells stably integrated with Flp-In constructs were cultured similarly, except the cell culture media were supplemented with 100 mg/L hygromycin B (Life Technologies) and no zeocin.

Stable cell line generation

Flp-In T-REx HEK293 cells were seeded at $1x10^5$ cells/mL in 2 mL (6-well plate) DMEM with 10% FBS. 24 hours later the cells were cotransfected with a pcDNA5/FRT-derived plasmid and pOG44 (Life Technologies) in a 1:9 ratio using FuGENE HD (Promega) according to the manufacturer's instructions. Typically DNA and FuGENE were incubated together in Opti-MEM in a 1:3:50 (g:L:L) ratio for approximately 1 hour, with 2 mL samples receiving 2 μg of DNA. 24 hours after transfection the cells were resuspended using 0.25% trypsin-EDTA and DMEM with 10% FBS, and ¼ of the cells were used to seed 2 mL (6-well plate) DMEM with 10% FBS. 24 hours later the media were replaced with DMEM with 10% FBS, 200 mg/L hygromycin B, and 5 mg/L blasticidin. The media were replaced every 72–96 hours until macroscopic colonies were visible, usually after 10–14 days. Colonies were pooled together with 0.25% trypsin-EDTA and passaged into DMEM with 10% FBS, 100 mg/L hygromycin B, and 5 mg/L blasticidin. 10% dimethyl sulfoxide (DMSO) stocks were made from resuspended cells, cooled by 1 degree/minute to −80°C, then stored at −320°C.

Transient transfection

Flp-In T-REx HEK293 cells were seeded at $1x10^5$ cells/mL in 500 μL (24-well plate), 10 mL (10 cm dish), or 400 μL (8-chambered coverglass) DMEM with 10% FBS. 21–27 hours (flow cytometry assay) or 48 hours (cellular fractionation and extraction) or 24 hours (confocal microscopy) after seeding the cells were transfected with one or two plasmids using FuGENE HD (Promega) or Lipofectamine 2000 (Life Technologies) according to the manufacturer's instructions. Typically DNA and FuGENE HD were

incubated together in Opti-MEM in a 1:3:50 (g:L:L) ratio for 1 approximately hour, while DNA and Lipofectamine were incubated together in Opti-MEM in a 1:2:100 (g:L:L) ratio for 5 minutes. With either transfection reagent, 500 μL samples received 500 ng of DNA, 10 mL samples received 10 μg of DNA, and 400 μL samples received 400 ng of DNA.

Flow cytometry

18–28 hours after seeding (30–75 minutes after transfection if applicable) doxycycline was added to derepress the CMV-TetO_2 promoter. 24–26 hours after transfection with plasmids encoding NF-κB- or β-catenin-responsive ribozyme switch designs inducer molecules were added. 10 μg/L TNFα (Sigma-Aldrich), 500 μg/L LPS (Sigma-Aldrich), or 500 μg/L LPS in combination with 10 mg/L cycloheximide (Sigma-Aldrich) were used to induce the NF-κB pathway, and 200 μg/L Wnt3A (R&D Systems) was used to induce the Wnt pathway. 42-52 hours after transfection fluorescence data were obtained by flow cytometry using the MACSQuant VYB equipped with 405 nm, 488 nm, and 561 nm lasers (Miltenyi Biotec). Viability was gated by side scatter and electronic volume, and viable cells were further gated for either DsRed, GFP, or BFP expression, which served as transfection controls. DsRed, GFP, and BFP fluorescence was measured through 615/20 nm, 525/50 nm, and 450/50 nm band-pass filters, respectively. Data were analyzed using FlowJo (Tree Star Inc.). Geometric mean values from biological replicates were reported with an error range of ±1 standard deviation. Geometric mean fluorescence values were normalized to those of a control with no ribozyme or the inactive ribozyme sTRSVctrl.

Cellular fractionation and extraction

1–1.5 hours before transfection cell culture media were replaced with media containing 1 mg/L doxycycline to derepress the CMV-TetO_2 promoter. 50 hours later cytoplasmic and nuclear extracts were prepared using the CelLytic NuCLEAR Extraction Kit (Sigma) with isotonic lysis buffer and IGEPAL CA-630 detergent according to the manufacturer's instructions, although modifications were made to the protocol to minimize cross-contamination between the nuclear and cytoplasmic fractions. Briefly, cells were washed with PBS, scraped off of the culture dishes, and centrifuged at 500 x g for 5 minutes. Packed cells were resuspended in isotonic lysis buffer and incubated for 1 minute on ice, then incubated with IGEPAL CA-630 at a final concentration of 0.04% on ice for 3 minutes. Lysed cells were centrifuged at 5000 x g for 30 seconds and the cytoplasmic fraction (supernatant) was collected. The pelleted nuclei were washed with isotonic lysis buffer and 0.04% IGEPAL CA-630, then centrifuged at 5000 x g for 30 seconds. The pelleted nuclei were resuspended in extraction buffer and agitated at 4°C for 30 minutes. Lysed nuclei were centrifuged at 18000 x g for 10 minutes and the nuclear fraction (supernatant) was collected.

Immunoblotting

A standard Bradford assay using Protein Assay reagent (Bio-Rad Laboratories) was performed with a BSA standard to determine protein concentrations. Samples were run on NuPAGE 4–12% Bis-Tris Gels (Life Technologies) in NuPAGE MOPS buffer (Life Technologies) at 150 V for 1 hour. Transfer was performed with extra thick blot paper (Bio-Rad Laboratories) and 0.45 μm Protran nitrocellulose transfer membrane

(Whatman) in 2x NuPAGE transfer buffer (Life Technologies) and 20% methanol using a Trans-Blot SD Semi-Dry Transfer Cell (Bio-Rad Laboratories) at 15 V for 15 minutes. Membranes were blocked with TBST (20 mM Tris, 137 mM sodium chloride, 0.1% Tween-20) and 5% bovine serum albumin (BSA) (Calbiochem) at room temperature for 1 hour, then rinsed with TBST twice for 5 minutes each. Membranes were probed with rabbit anti-enterobacteriophage MS2 coat protein, anti-GAPDH, and anti-HDAC1 polyclonal antibodies (Millipore) in TBST and 1% BSA at 4°C for 16 hours, then rinsed with TBST twice for 5 minutes each. Membranes were probed with sheep anti-rabbit IgG, horseradish peroxidase (HRP) conjugate polyclonal antibody (Millipore) at room temperature for 1 hour, then rinsed with TBST twice for 5 minutes each. HRP signal was detected using SuperSignal West Pico Chemiluminescent Substrate (Thermo Scientific) according to the manufacturer's instructions and a G:Box Chemi XT4 imaging system (Syngene). Band intensity was calculated with GeneTools software (Syngene).

Immunofluorescence microscopy

Flp-In T-REx HEK293 cells with stably integrated 2MS2mut constructs were seeded at $1x10^5$ cells/mL in 1 mL (4-chambered coverglass) DMEM with 10% FBS, 100 mg/L hygromycin B, and 1 mg/L doxycycline to derepress the CMV-$TetO_2$ promoter. Approximately 43 hours after seeding cells were washed with phosphate buffered saline (PBS) (Life Technologies) and fixed for 15–20 minutes using HistoChoice MB tissue fixative (AMRESCO). Cells were washed twice with PBS, blocked with PBS and 1.5% BSA for 1 hour, and washed with PBS for 5 minutes. Cells were probed with rabbit anti-enterobacteriophage MS2 coat protein at 4°C for approximately 17 hours, then washed

with PBS for 5 minutes. Cells were probed with sheep anti-rabbit fluorescein conjugated [$F(ab')_2$ fragments] polyclonal antibody (Chemicon) for 30 minutes, then washed thrice with PBS for 5 minutes each. Cell nuclei were counterstained using 250 μg/L 7-AAD (Life Technologies) in PBS for 5 minutes, then washed with PBS. Cells were imaged on a Zeiss Axiovert 200M fluorescence microscope (Zeiss) with a 20x objective using the AxioVision software (Zeiss). Images were exported and brightness and contrast were adjusted using FIIJ.

Confocal fluorescence microscopy

Approximately 30 minutes after transfection 1 mg/L doxycycline was added to derepress the CMV-$TetO_2$ promoter, and 23 hours later media were replaced with media containing 1 mg/L doxycycline. 24 hours later cell nuclei were counterstained using 250 nM SYTO 16 (Life Technologies). 24 hours after counterstaining cells were imaged on a Leica TCS SP8 confocal microscope (Leica Microsystems) with a 20x objective using the Leica Application Suite Advanced Fluorescence software (Leica Microsystems). Images were exported and brightness and contrast were adjusted using FIIJ.

Acknowledgements

We thank Andrew Kennedy and Leopold d'Espaux for designing ribozyme switches, designing experiments, and evaluating results; Marty Bigos for help evaluating flow cytometry results; Kitty Lee and the Stanford Cell Sciences Imaging Facility for providing fluorescence microscopy access and training; Stephanie Culler, Rachel Green,

Louis Maher III, and Melina Mathur for providing plasmid constructs; and Ryan Bloom and Melina Mathur for providing stable cell lines with integrated constructs. This work was supported by the National Institutes of Health (grant to Christina Smolke, RC1GM091298) and the Defense Advanced Research Projects Agency (grant to Christina Smolke, HR0011-11-2-0002).

References

1. Chang, A. L. et al. Synthetic RNA switches as a tool for temporal and spatial control over gene expression. Curr. Opin. Biotechnol. **23,** 679–688 (2012).

2. Nie, M. & Htun, H. Different modes and potencies of translational repression by sequence-specific RNA-protein interaction at the 5'-UTR. Nucleic Acids Res. **34,** 5528–5540 (2006).

3. Ausländer, S. et al. Programmable single-cell mammalian biocomputers. Nature **487,** 123–127 (2012).

4. Saito, H. et al. Synthetic translational regulation by an L7Ae-kink-turn RNP switch. Nat. Chem. Biol. **6,** 71–78 (2010).

5. Stapleton, J. a. et al. Feedback Control of Protein Expression in Mammalian Cells by Tunable Synthetic Translational Inhibition. ACS Synth. Biol. **1,** 83–88 (2012).

6. Endo, K. et al. Quantitative and simultaneous translational control of distinct mammalian mRNAs. Nucleic Acids Res. **41,** e135 (2013).

7. Liu, Y. et al. Synthesizing oncogenic signal-processing systems that function as both "signal counters" and "signal blockers" in cancer cells. Mol. Biosyst. **9,** 1909–1918 (2013).

8. Endo, K. et al. A versatile cis-acting inverter module for synthetic translational switches. Nat. Commun. **4,** 2393 (2013).

9. Saito, H. et al. Synthetic human cell fate regulation by protein-driven RNA switches. Nat. Commun. **2,** 160 (2011).

10. Culler, S. J. et al. Reprogramming cellular behavior with RNA controllers responsive to endogenous proteins. Science. **330,** 1251–1255 (2010).

11. Win, M. N. & Smolke, C. D. A modular and extensible RNA-based gene-regulatory platform for engineering cellular function. Proc. Natl. Acad. Sci. U. S. A. **104,** 14283–14288 (2007).

12. Michener, J. K. & Smolke, C. D. High-throughput enzyme evolution in Saccharomyces cerevisiae using a synthetic RNA switch. Metab. Eng. **14,** 306–316 (2012).

13. Galloway, K. E. et al. Dynamically reshaping signaling networks to program cell fate via genetic controllers. Science. **341,** 1235005 (2013).

14. Ausländer, S. et al. A ligand-dependent hammerhead ribozyme switch for controlling mammalian gene expression. Mol. Biosyst. **6,** 807–814 (2010).

15. Chen, Y. Y. et al. Genetic control of mammalian T-cell proliferation with synthetic RNA regulatory systems. Proc. Natl. Acad. Sci. U. S. A. **107,** 8531–8536 (2010).

16. Wieland, M. et al. Engineering of ribozyme-based riboswitches for mammalian cells. Methods **56,** 351–357 (2012).

17. Wei, K. Y. et al. A yeast-based rapid prototype platform for gene control elements in mammalian cells. Biotechnol. Bioeng. **110,** 1201–1210 (2013).

18. Stripecke, R. et al. Proteins binding to 5'untranslated region sites: a general mechanism for translational regulation of mRNAs in human and yeast cells. Mol. Cell. Biol. **14,** 5898–5909 (1994).

19. Paraskeva, E. et al. A translational repression assay procedure (TRAP) for RNA-protein interactions in vivo. Proc. Natl. Acad. Sci. U. S. A. **95,** 951–956 (1998).

20. Fusco, D. et al. Single mRNA molecules demonstrate probabilistic movement in living mammalian cells. Curr. Biol. **13,** 161–167 (2003).

21. Hobson, D. & Uhlenbeck, O. C. Alanine scanning of MS2 coat protein reveals protein-phosphate contacts involved in thermodynamic hot spots. J. Mol. Biol. **356,** 613–624 (2006).

22. Keryer-Bibens, C. et al. Tethering of proteins to RNAs by bacteriophage proteins. Biol. Cell **100,** 125–138 (2008).

23. Khvorova, A. et al. Sequence elements outside the hammerhead ribozyme catalytic core enable intracellular activity. Nat. Struct. Biol. **10,** 708–712 (2003).

24. Li, X. et al. Generation of Destabilized Green Fluorescent Protein as a Transcription Reporter. J. Biol. Chem. **273,** 34970–34975 (1998).

25. Beckett, D. & Uhlenbeck, O. C. Ribonucleoprotein complexes of R17 coat protein and a translational operator analog. J. Mol. Biol. **204,** 927–938 (1988).

26. Sugiyama, T. et al. Ribonucleoprotein Complexes formed between Bacteriophage MS2 RNA and MS2 Protein in vitro. J. Mol. Biol. **25,** 455–463 (1967).

27. LeCuyer, K. A. et al. Mutants of the bacteriophage MS2 coat protein that alter its cooperative binding to RNA. Biochemistry **34,** 10600–10606 (1995).

28. Peabody, D. S. & Lim, F. Complementation of RNA binding site mutations in MS2 coat protein heterodimers. Nucleic Acids Res. **24,** 2352–2359 (1996).

29. Wang, R. & Brattain, M. G. The maximal size of protein to diffuse through the nuclear pore is larger than 60kDa. FEBS Lett. **581,** 3164–3170 (2007).

30. Kalderon, D. et al. A short amino acid sequence able to specify nuclear location. Cell **39,** 499–509 (1984).

31. Wen, W. et al. Identification of a signal for rapid export of proteins from the nucleus. Cell **82,** 463–473 (1995).

32. Lim, F. et al. Translational repression and specific RNA binding by the coat protein of the Pseudomonas phage PP7. J. Biol. Chem. **276,** 22507–22513 (2001).

33. Tan, R. & Frankel, A. D. Structural variety of arginine-rich RNA-binding peptides. Proc. Natl. Acad. Sci. U. S. A. **92,** 5282–5286 (1995).

34. Karin, M. et al. NF-κB in cancer: from innocent bystander to major culprit. Nat. Rev. Cancer **2,** 301–310 (2002).

35. Lessard, L. et al. NF-κB nuclear localization and its prognostic significance in prostate cancer. BJU Int. **91,** 417–420 (2003).

36. Kontos, S. et al. Inverse expression of estrogen receptor-beta and nuclear factor-κB in urinary bladder carcinogenesis. Int. J. Urol. **17,** 801–809 (2010).

37. Koga, F. et al. ErbB2 and NFκB overexpression as predictors of chemoradiation resistance and putative targets to overcome resistance in muscle-invasive bladder cancer. PLoS One **6,** e27616 (2011).

38. Kau, T. R. et al. Nuclear transport and cancer: from mechanism to intervention. Nat. Rev. Cancer **4,** 106–117 (2004).

39. Lebruska, L. L. & Maher, L. J. Selection and characterization of an RNA decoy for transcription factor NF-κB. Biochemistry **38,** 3168–3174 (1999).

40. Wurster, S. & Maher, L. Selection and characterization of anti-NF-κB p65 RNA aptamers. RNA **14,** 1037–1047 (2008).

41. Lee, H. K. et al. Modulation of oncogenic transcription and alternative splicing by beta-catenin and an RNA aptamer in colon cancer cells. Cancer Res. **66,** 10560–10566 (2006).

42. Choi, Y. S. et al. The RNA aptamer disrupts protein-protein interaction between beta-catenin and nuclear factor-κB p50 and regulates the expression of C-reactive protein. FEBS Lett. **583,** 1415–1421 (2009).

43. Hogg, J. & Collins, K. RNA-based affinity purification reveals 7SK RNPs with distinct composition and regulation. RNA **13,** 868–880 (2007).

44. Ganchi, P. A. et al. IκB/MAD-3 Masks the Nuclear Localization Signal of NF-κB p65 and Requires the Transactivation Domain to Inhibit NF-κB p65 DNA Binding. Mol. Biol. Cell **3,** 1339–1352 (1992).

45. Huxford, T. et al. The Crystal Structure of the IκBα/NF-κB Complex Reveals Mechanisms of NF-κB Inactivation. Cell **95,** 759–770 (1998).

46. Huang, D.-B. et al. Crystal structure of NF-κB (p50)2 complexed to a high-affinity RNA aptamer. Proc. Natl. Acad. Sci. U. S. A. **100,** 9268–9273 (2003).

47. Ghosh, G. et al. NF-κB regulation: lessons from structures. Immunol. Rev. **246,** 36–58 (2012).

48. Lee, H. K. & Jeong, S. β-Catenin stabilizes cyclooxygenase-2 mRNA by interacting with AU-rich elements of 3'-UTR. Nucleic Acids Res. **34,** 5705–5714 (2006).

49. Kim, I. et al. β-Catenin recognizes a specific RNA motif in the cyclooxygenase-2 mRNA 3'-UTR and interacts with HuR in colon cancer cells. Nucleic Acids Res. **40,** 6863–6872 (2012).

50. Liang, J. C. et al. A high-throughput, quantitative cell-based screen for efficient tailoring of RNA device activity. Nucleic Acids Res. **40,** e154 (2012).

51. Daugherty, P. S. et al. Flow cytometric screening of cell-based libraries. J. Immunol. Methods **243,** 211–227 (2000).

52. Kosuri, S. et al. Composability of regulatory sequences controlling transcription and translation in Escherichia coli. Proc. Natl. Acad. Sci. U. S. A. **110,** 14024–14029 (2013).

53. Beisel, C. L. et al. Model-guided design of ligand-regulated RNAi for programmable control of gene expression. Mol. Syst. Biol. **4,** (2008).

54. Beisel, C. L. et al. Design of small molecule-responsive microRNAs based on structural requirements for Drosha processing. Nucleic Acids Res. **39,** 2981–2994 (2011).

55. Gibson, D. G. et al. Enzymatic assembly of DNA molecules up to several hundred kilobases. Nat. Methods **6,** 343–345 (2009).

56. Mathews, D. H. Using an RNA secondary structure partition function to determine confidence in base pairs predicted by free energy minimization. RNA **10,** 1178–1190 (2004).

Supplementary Tables

Supplementary Table 3.1. DNA sequences of RNA devices.

RNA device	ligand	DNA sequence
sTRSV	N/A	GCTGTCACCGGATGTGCTTTCCGGTCTGATGAGTCCGTGAGGACGAAACAGC
sTRSVctrl	N/A	GCTGTCACCGGATGTGCTTTCCGGTCTGATGAGTCCGTGAGGACAAAACAGC
MS2-A1	MS2 coat protein	GCTGTCACCGGACTACACCATCAGGGTAGTGTGCTTTCCGGTCTGATGAGTCCGTGAGGACGAAACAGC
MS2-A2	MS2	GCTGTCACCGGATGTGCGTACACCATCAGGGTACTTTCCGGTCTGATGAGTCCGTGAGGACGAAACAGC
MS2-A3	MS2	GCTGTCACCGGATGTGCTTTCCGGTCTGATGAGTCCGTCGTACACCATCAGGGTACGGAGGACGAAACAGC
MS2-A4	MS2	GCTGTCACCGGATGTGGTTTCCGGTCTGATGAGTCCGTCGTACACCATCAGGGTACGGAGGACGAAACAGC
MS2-A5	MS2	GCTGTCACCGGAATCAAGGTCCGGTCTGATGAGTCCGTCGTACACCATCAGGGTACGGAGGACGAAACAGC
MS2-A6	MS2	GCTGTCACCGGATTCGGGATCCGGTCTGATGAGTCCGTCGTACACCATCAGGGTACGGAGGACGAAACAGC
MS2-A7	MS2	GCTGTCACCGGATGTGCTTTCCGGTCTGATGAGTCCGTGCGTACACCATCAGGGTACGAGGACGAAACAGC
MS2-B1	MS2	GCTGTCACCGGATGTGCTTTCCGGTCTGATGAGTCCGTTGTCCAGGATCACCGGACGGGACGGAGGACGAAACAGC
MS2-B2	MS2	GCTGTCACCGGAATCAAGGTCCGGTCTGATGAGTCCGTTGTCCACCATCAGGGGACGGGACGGAGGACGAAACAGC
MS2-B2ctrl	MS2	GCTGTCACCGGAATCAAGGTCCGGTCTGATGAGTCCGTTGTCCACCATCAGGGGACGGGACGGAGGACAAAACAGC
MS2-B3	MS2	GCTGTCACCGGATGTGCTTTCCGGTCTGATGAGTCCGTGGTCCACCATCAGGGGACTGGACTGAGGACGAAACAGC
MS2-B4	MS2	GCTGTCACCGGATGTGCTTTCCGGTCTGATGAGTCCGTCGTCCAGGATCACCGGACGGGACGGAGGACGAAACAGC

MS2-B5	MS2	GCTGTCACCGGATGTGCTTTCCGGTCTGATGAGT CCGTCGTCCTAGGATCACCAGGACGGGACGGAG GACGAAACAGC
MS2-B6	MS2	GCTGTCACCGGATGTGCTTTCCGGTCTGATGAGT CCGTCGTCCTAGGATCACCAGGAAGGGACGGAG GACGAAACAGC
MS2-B7	MS2	GCTGTCACCGGATGTGCTTTCCGGTCTGATGAGT CCGTTGTCCTAGGATCACCAGGAAGGGACGGAG GACGAAACAGC
MS2-B8	MS2	GCTGTCACCGGATGTGCTTTCCGGTCTGATGAGT CCGTTGCGTAGGATCACCACGTGGCGCGGAGGAC GAAACAGC
MS2-B9	MS2	GCTGTCACCGGATGTGCTTTCCGGTCTGATGAGT CCGTTGTAGGATCACCACACGGAGGACGAAACA GC
MS2-B10	MS2	GCTGTCACCGGAATCAAGGTCCGGTCTGATGAGT CCGTGGTCCACCATCAGGGGACTGGACTGAGGAC GAAACAGC
MS2-B11	MS2	GCTGTCACCGGAATCAAGGTCCGGTCTGATGAGT CCGTTGTCCTAGGATCACCAGGAAGGGACGGAG GACGAAACAGC
MS2-C1	MS2	GCTGTCACCGGATGTGCTGCAGGATCACCGCATT TCCGGTCTGATGAGTCCGTGAGGACGAAACAGC
MS2-C1ctrl	MS2	GCTGTCACCGGATGTGCTGCAGGATCACCGCATT TCCGGTCTGATGAGTCCGTGAGGACAAAACAGC
MS2-C2	MS2	GCTGTCACCGGATGTGGTTTCCGGTCTGATGAGT CCGACCATCAGGAGGACGAAACAGC
MS2-C3	MS2	GCTGTCACCGGAATCAAGGTCCGGTCTGATGAGT CCGACCATCAGGAGGACGAAACAGC
MS2-C3ctrl	MS2	GCTGTCACCGGAATCAAGGTCCGGTCTGATGAGT CCGACCATCAGGAGGACAAAACAGC
MS2-C4	MS2	GCTGTCACCGGATTCGGGATCCGGTCTGATGAGT CCGACCATCAGGAGGACGAAACAGC
MS2-D1	MS2	TGCTGTACGATCACGACAGCGGGCTAAAGCCCGC TGTCACCGGATGTGCTTTCCGGTCTGATGAGTCC GTGAGGACGAAACAGCGGGCC
MS2-D2	MS2	TGCTGCACGATCACGGCAGCGAGCTAAAGCTCGC TGTCACCGGATGTGCTTTCCGGTCTGATGAGTCC GTGAGGACGAAACAGCGGGCC
MS2-D3	MS2	TGCTGCAGGATCACCGCAGCGAGCTAAAGCTCGC TGTCACCGGATGTGCTTTCCGGTCTGATGAGTCC GTGAGGACGAAACAGCGAC
MS2-D4	MS2	TGCTTCATGATCACAGGAGCGGCACTAAAGTGCC GCTGTCACCGGATGTGCTTTCCGGTCTGATGAGT CCGTGAGGACGAAACAGCGGGCC

MS2-D5	MS2	TAAAATAGTCATGATCACAGGCTGTCACCGGATG TGCTTTCCGGTCTGATGAGTCCGTGAGGACGAAA CAGCCC
MS2-D6	MS2	TAAAATAGTTAGGATCACCGGCTGTCACCGGATG TGCTTTCCGGTCTGATGAGTCCGTGAGGACGAAA CAGCCC
PP7-1	PP7 coat protein	GCTGTCACCGGAATCAAGGTCCGGTCTGATGAGT CCGAGTTTATATGGAAACAGGACGAAACAGC
PP7-2	PP7	GCTGTCACCGGAATCAAGGTCCGGTCTGATGAGT CCGTGTTATATGGAACGGGACGAAACAGC
PP7-3	PP7	GCTGTCACCGGAATCAAGGTCCGGTCTGATGAGT CCGTTGGTATATGGACCGGGGACGAAACAGC
Lambda-1	Lambda N 1-22 peptide	GCTGTCACCGGAATCAAGGTCCGGTCTGATGAGT CCGTTGTCCGAAGAGGACGGGACGGAGGACGAA ACAGC
Lambda-2	Lambda N	GCTGTCACCGGAATCAAGGTCCGGTCTGATGAGT CCGTTGTCCTGAAGAAGGAAGGGACGGAGGACG AAACAGC
Lambda-3	Lambda N	GCTGTCACCGGAATCAAGGTCCGGTCTGATGAGT CCGTAGAGGACGAAACAGC
Lambda-4	Lambda N	GCTGTCACCGGAATCAAGGTCCGGTCTGATGAGT CCTGTAGAAGGACGAAACAGC
p50-1	NF-κBp50	GCTGTCACCGGATGTGCTTTCCGGTCTGATGAGT CCGTTGGTATCCTGAAACTGTTATAAGGTTGGCC GATGTTGGAGGACGAAACAGC
p50-2	p50	GCTGTCACCGGAATCAAGGTCCGGTCTGATGAGT CCGTTGGTATCCTGAAACTGTTATAAGGTTGGCC GATGTTGGAGGACGAAACAGC
p50-3	p50	GCTGTCACCGGATGTGCTTTCCGGTCTGATGAGT CCGTGGGTATCCTGAAACTGTTATAAGGTTGGCC GATGTTGGAGGACGAAACAGC
p50-4	p50	GCTGTCACCGGAATCAAGGTCCGGTCTGATGAGT CCGTGGGTATCCTGAAACTGTTATAAGGTTGGCC GATGTTGGAGGACGAAACAGC
p50-5	p50	GCTGTCACCGGATGTGCTTTCCGGTCTGATGAGT CCGTTGGTATCCTGAAACTGTTATAAGGTTGGCC GATGTGTGGAGGACGAAACAGC
p50-6	p50	GCTGTCACCGGAATCAAGGTCCGGTCTGATGAGT CCGTTGGTATCCTGAAACTGTTATAAGGTTGGCC GATGTGTGGAGGACGAAACAGC
p50-7	p50	GCTGTCACCGGATGTGCTTTCCGGTCTGATGAGT CCGTTGTCCATCCTGAAACTGTTATAAGGTTGGC CGATGGACGGATGGACGGAGGACGAAACAGC
p50-8	p50	GCTGTCACCGGAATCAAGGTCCGGTCTGATGAGT CCGTTGTCCATCCTGAAACTGTTATAAGGTTGGC CGATGGACGGATGGACGGAGGACGAAACAGC

p50-9	p50	GCTGTCACCGGATGTGCTTTCCGGTCTGATGAGT CCGTTGTCCATCCTGAAACTGTTATAAGGTTGGC CGATGGACAGATGGACGGAGGACGAAACAGC
p50-10	p50	GCTGTCACCGGAATCAAGGTCCGGTCTGATGAGT CCGTTGTCCATCCTGAAACTGTTATAAGGTTGGC CGATGGACAGATGGACGGAGGACGAAACAGC
p50-11	p50	GCTGTCACCGGATGTGCTTTCCGGTCTGATGAGT CCGTCATCCTGAAACTGTTATAAGGTTGGCCGAT GGGGACGGAGGACGAAACAGC
p50-12	p50	GCTGTCACCGGATGTGCTTTCCGGTCTGATGAGT CCGTGTCCTTGAAACTGTAAGGTTGGCGGACGGG ACGAGGACGAAACAGC
p50-13	p50	GCTGTCACCGGATGTGCTTTCCGGTCTGATGAGT CCGTCATCCTGAAACTGTTATAAGGTTGGCCGAT GGGGACGAGGACGAAACAGC
p65-1	NF-κBp65	GCTGTCACCGGATGTGCTCGATGAGTCCGCGAGG TGCCGAACCTCCATTGGGGTCGGTTTCCGGTCTG ATGAGTCCGTGAGGACGAAACAGC
p65-2	p65	GCTGTCACCGGATGTGCTTTCCGGTCTGATGAGT CCGTTTGATTCGATGAGTCCGCGAGGTGCCGAAC CTCCATTGGGGTCGAGAGGACGAAACAGC
p65-3	p65	GCTGTCACCGGAATCAAGGTCCGGTCTGATGAGT CCGTTTGATTCGATGAGTCCGCGAGGTGCCGAAC CTCCATTGGGGTCGAGAGGACGAAACAGC
p65-4	p65	GCTGTCACCGGATGTGCTTTCCGGTCTGATGAGT CCGTTTGATCGATGAGTCCGCGAGGTGCCGAACC TCCATTGGGGTCGAGAGGACGAAACAGC
p65-5	p65	GCTGTCACCGGAATCAAGGTCCGGTCTGATGAGT CCGTTTGATCGATGAGTCCGCGAGGTGCCGAACC TCCATTGGGGTCGAGAGGACGAAACAGC
Bcat-A1	β-catenin	GACGTATGAGACTATGGACGCTATAGGCACACCG GATACTTTAACGTCTCACTGATGAGGCCATGGCA GGCCGAAACGTC
Bcat-A2	β-catenin	TACGTCTGAGCGTATGGACGCTATAGGCACACCG GATACTTTAACCGCTCACTGAAGATGGCCCGGTA GGGCCGAAACGTA
Bcat-A3	β-catenin	AAGAGGTCGGCACCTATGGACGCTATAGGCACA CCGGATACTTTAACGGTGTCCTGATGAAGATCCA TGACAGGATCGAAACCTCTT
Bcat-A4	β-catenin	CGCTGTCTGTACTTATGGACGCTATAGGCACACC GGATACTTTAACAGTACACTGACGAGTCCCTAAA GGACGAAACAGCG
Bcat-B1	β-catenin	GGCCGATCTATGGACGCTATAGGCACACCGGATA CTTTAACGATTGGCTATAAAAGCTGTCACCGGAT GTGCTTTCCGGTCTGATGAGTCCGTGAGGACGAA ACAGCC

Bcat-B2	β-catenin	GCCGATCTATGGACGCTATAGGCACACCGGATAC TTTAACGATTGGCATAAAAGCTGTCACCGGATGT GCTTTCCGGTCTGATGAGTCCGTGAGGACGAAAC AGCC
Bcat-B3	β-catenin	TAGGCCGATCTATGGACGCTATAGGCACACCGGA TACTTTAACGATTGGCTAAAAGCTGTCACCGGAT GTGCTTTCCGGTCTGATGAGTCCGTGAGGACGAA ACAGCC
Bcat-B4	β-catenin	TAAGCCGATCTATGGACGCTATAGGCACACCGGA TACTTTAACGATTGGCAAAGCTGTCACCGGATGT GCTTTCCGGTCTGATGAGTCCGTGAGGACGAAAC AGCC
Bcat-B5	β-catenin	TAAAAACCAGCATCTATGGACGCTATAGGCACAC CGGATACTTTAACGATGCTGTCACCGGATGTGCT TTCCGGTCTGATGAGTCCGTGAGGACGAAACAGC ATC
Bcat-B6	β-catenin	TAAAATCGCCGATCTATGGACGCTATAGGCACAC CGGATACTTTAACGATTGGCTCACCGGATGTGCT TTCCGGTCTGATGAGTCCGTGAGGACGAAAGCCA

Supplementary Table 3.2. Free energies (ΔG, kcal/mol) of individual conformations (ribozyme cleavage-active and -inactive) and the energy difference (ΔΔG, kcal/mol) predicted by RNAstructure 5.3[56].

	aptamer unformed		**aptamer formed**		
RNA device	**active**	**inactive**	**inactive**	**active**	**inactive - active**
sTRSV	-19.3		N/A		N/A
sTRSVctrl		-19.3	N/A		N/A
MS2-A1	N/A			-23.2	N/A
MS2-A2	N/A			-24.5	N/A
MS2-A3	N/A			-31.1	N/A
MS2-A4	N/A			-31.1	N/A
MS2-A5	N/A			-30.2	N/A
MS2-A6	N/A			-32.4	N/A
MS2-A7	N/A			-27.1	N/A
MS2-B1	-27.7		-26.9		0.8
MS2-B2	-28.7		-27.3		1.4
MS2-B2ctrl		-28.7	-27.3		N/A
MS2-B3	-30.6		-29.1		1.5
MS2-B4	-29.7		-28.5		1.2

MS2-B5	-30.4		-30.3		0.1
MS2-B6	-30.4		-27.9		2.5
MS2-B7	-28.5		-26.1		2.4
MS2-B8	-27.4		-25.5		1.9
MS2-B9	-22.7		-21.6		1.1
MS2-B10	-29.7		-28.2		1.5
MS2-B11	-27.5		-25.2		2.3
MS2-C1		-24.6		-22.3	-2.3
MS2-C1ctrl		-24.6	-22.3		N/A
MS2-C2	-20.6		N/A		N/A
MS2-C3	-19.7		N/A		N/A
MS2-C3ctrl		-19.7	N/A		N/A
MS2-C4	-21.9		N/A		N/A
MS2-D1		-41.8		-40.7	-1.1
MS2-D2		-39.1		-39.8	0.7
MS2-D3		-36.2		-35.6	-0.6
MS2-D4		-34.7		-34.3	-0.4
MS2-D5	-23.6		-23.0		0.6
MS2-D6	-23.8		-22.5		1.3
PP7-1	-19.7		N/A		N/A
PP7-2	-19.6		N/A		N/A
PP7-3	-22.5		N/A		N/A
Lambda-1	-27.6		-25.2		2.4
Lambda-2	-28.2		-23.9		4.3
Lambda-3	-18.3		N/A		N/A
Lambda-4	-19.6		N/A		N/A
p50-1		-25.3		-24.8	-0.5
p50-2		-24.4		-23.9	-0.5
p50-3		-24.0		-23.7	-0.3
p50-4		-23.7		-23.4	-0.3
p50-5		-25.1		-23.0	-2.1
p50-6		-24.8		-22.7	-2.1
p50-7	-38.0		-36.3		1.7
p50-8	-37.7		-36.0		1.7
p50-9	-36.8		-36.2		0.6
p50-10	-36.5		-35.9		0.6
p50-11	-27.8		-26.1		1.7
p50-12	-30.5		-28.3		2.2
p50-13	-26.8		-26.1		0.7
p65-1		-35.0		-34.4	-0.6
p65-2	-36.0		-33.7		2.3

p65-3	-35.1		-32.8		2.3
p65-4	-34.3		-34.1		0.2
p65-5	-33.4		-33.2		0.2
Bcat-A1	-21.0		N/A		N/A
Bcat-A2	-23.5		N/A		N/A
Bcat-A3	-23.8		N/A		N/A
Bcat-A4	-18.2		N/A		N/A
Bcat-B1		-31.3		-31.9	0.6
Bcat-B2		-30.3		-31.3	1.0
Bcat-B3		-33.1		-32.2	-0.9
Bcat-B4		-30.9		-31.3	0.4
Bcat-B5	-29.7		-28.8		0.9
Bcat-B6	-27.2		-25.9		1.3

Supplementary Table 3.3. Primer and oligonucleotide sequences.

Name	**DNA Sequence**
5'spacer	AATAAATAAAA
3'spacer	CAAATAAACAAACACTC
S 5'spacer	AATAAA
S 3'spacer	AAATAAACAAACACTC
lambda N	TCGAGATGGACGCCCAGACCAGAAGGAGAGAGAGGAG AGCCGAGAAGCAGGCCCAGTGGAAGGCCGCCAACTAG CGGC
insertNA	CTGGCTAAAGGTGCGT
No NLS A/X Fwd	CAACTCGAGATGGTGGCTTCTAACTTTACTCAG
DsRed A/X Rev	CAAGGGCCCGCCGCTACTGGGAGC
MS2 A/X Rev	CAAGGGCCCGCCGCTAGTAGATGCCG
EF1BFP Fwd	CAAAGATCTGGATCTGCGATCGC
EF1BFP Rev	CAACCTAGGTCAATTAAGCTTGTGCCCCAG
MS2 NotI F	CAAGCGGCCGCTCGAGATGGCTTCTAACTTTACTCAGTT CGTTCTC
MS2 ApaI R	CAAGGGCCCGCCGCTAGTAGATGCCGGAGTTTGCT
NLS MS2 F	CAAGCGGCCGCTCGAGATGCCAAAGAAGAAGCGCAAA GTGGCTTCTAACTTTACTCAGTTCGTTCTC
2MS2mut R	AGCGGGTTTAAACGGGCCCGCCGCTA
2MS2mut F	GCAGATATCCAGCACAGTGGCGGCCGCTCGAGATG

NES MS2 R	CAAGGGCCCGCCGCTAGATGTCCAGTCCGGCCAGCTTC AGGGCCAGCTCGTTGTAGATGCCGGAGTTTGCT
DsRed GF	CCCGATTCCCTCGGCAATCGCAGCAAACTCCGGCATCT ACG
DsRed NES R	AACTAGAAGGCACAGTCGAGGCTGATCAGCGGGTTTAA ACGGGCCCGCCGCTAGATGTCCAGTCCGGCCAGCTTCA GGGCCAGCTCGTTCTGGGAGCCGGAGTG
DsRed GR	AACTAGAAGGCACAGTCGAGG
GF Clover	CCTCGAGTATTCGCCACCATGGTGAGCAAGGGCG
GR Clover	GCGCGCCTTACCTAGGTTACTTGTACAGCTCGTCCATGC
GF EF1	GCATGGACGAGCTGTACAAGTAACCTAGGTAAGGCGCG C
GR EF1	CGCCCTTGCTCACCATGGTGGCGAATACTCGAGG
PP7 NotI F	CAAGCGGCCGCTCGAGATGGCCAAAACCATCGTTCT
PP7 ApaI R	CAAGGGCCCGCCGCTAGGAACGGCCCAGCG
p50 NotI F	CAAGCGGCCGCTCGAGATGGCAGAAGATGATCCATATT TGGGAAG
p50 ApaI R	CAAGGGCCCGCCGCTAGTCATCACTTTTGTCACAACCTT CA
p65 NotI F	CAAGCGGCCGCTCGAGATGGACGATCTGTTTCCCCT
p65 ApaI R	CAAGGGCCCGCCGCTAGGTCCTTTTCGCCTTCTCTTC
b-cat NotI F	CAAGCGGCCGCTCGAGATGCGTGCAATCCCTGAACTGA
b-cat ApaI R	CAAGGGCCCGCCGCTACTTGTCCTCAGACATTCGGAAC

Supplementary Table 3.4. Plasmid constructs.

Plasmid	**Description**
pCS2304	pcDNA5/FRT with d2EGFP, bGHpA, and CMV-TetO2 inserted between AflII/KpnI
pCS2359	pCS2304 with MS2-DsRedMonomer fusion protein inserted between XhoI/ApaI
pCS2394	pCS2359 with sTRSV with spacers inserted between AvrII/AscI
pCS2380	pCS2359 with MS2-A1 with spacers inserted between AvrII/AscI
pCS2381	pCS2359 with MS2-A2 with spacers inserted between AvrII/AscI
pCS2382	pCS2359 with MS2-A5 with spacers inserted between AvrII/AscI

pCS2383	pCS2359 with MS2-A6 with spacers inserted between AvrII/AscI
pCS2406	pCS2359 with d2EGFP removed from NheI/AvrII
pCS2409	pCS2406 with MS2 inserted between XhoI/ApaI
pCS1	blank plasmid with no mammalian promoters (Maung Win)
pCS339	pcDNA3.1(+) with chloramphenicol acetyltransferase (Chase Beisel)
pCS1392	pcDNA5/FRT with FLAG-NLS-MS2-DsRedMonomer (Stephanie Culler)
pCS2585	pcDNA5/FRT with EF1α-BFP-HSVTK (Melina Mathur)
pCS2595	pCS2304 with EF1α-BFP inserted between BglII/AvrII and MS2 inserted between XhoI/ApaI
pCS2602	pCS2595 with sTRSVctrl with spacers inserted between AvrII/AscI
pCS2601	pCS2595 with sTRSV with spacers inserted between AvrII/AscI
pCS2615	pCS2595 with MS2-B1 with spacers inserted between AvrII/AscI
pCS2616	pCS2595 with MS2-B2 with spacers inserted between AvrII/AscI
pCS1697	pCS2595 with MS2-B2ctrl with spacers inserted between AvrII/AscI
pCS2621	pCS2595 with MS2-B3 with spacers inserted between AvrII/AscI
pCS2610	pCS2595 with MS2-B4 with spacers inserted between AvrII/AscI
pCS2611	pCS2595 with MS2-B6 with spacers inserted between AvrII/AscI
pCS2612	pCS2595 with MS2-B7 with spacers inserted between AvrII/AscI
pCS2613	pCS2595 with MS2-B8 with spacers inserted between AvrII/AscI
pCS2614	pCS2595 with MS2-B9 with spacers inserted between AvrII/AscI
pCS2617	pCS2595 with MS2-C1 with spacers inserted between AvrII/AscI
pCS1698	pCS2595 with MS2-C1ctrl with spacers inserted between AvrII/AscI
pCS2618	pCS2595 with MS2-C2 with spacers inserted between AvrII/AscI
pCS2619	pCS2595 with MS2-C3 with spacers inserted between AvrII/AscI
pCS2385	pCS2595 with MS2-C3ctrl with spacers inserted between AvrII/AscI

pCS2620	pCS2595 with MS2-C4 with spacers inserted between AvrII/AscI
pCS2595+MS2-D1	pCS2595 with MS2-D1 with S spacers inserted between AvrII/AscI
pCS2595+MS2-D2	pCS2595 with MS2-D2 with S spacers inserted between AvrII/AscI
pCS2606	pCS2595 with MS2-D3 with S spacers inserted between AvrII/AscI
pCS2607	pCS2595 with MS2-D4 with S spacers inserted between AvrII/AscI
pCS2608	pCS2595 with MS2-D5 with S spacers inserted between AvrII/AscI
pCS2609	pCS2595 with MS2-D6 with S spacers inserted between AvrII/AscI
pCS2631	pCS2595 with MS2mut inserted between NotI/ApaI
pCS2632	pCS2631 with MS2-B1 with spacers inserted between AvrII/AscI
pCS2633	pCS2631 with MS2-B2 with spacers inserted between AvrII/AscI
pCS2650	pCS2631 with MS2-B3 with spacers inserted between AvrII/AscI
pCS2651	pCS2631 with MS2-B7 with spacers inserted between AvrII/AscI
pCS2634	pCS2631 with MS2-C1 with spacers inserted between AvrII/AscI
pCS2635	pCS2631 with MS2-C3 with spacers inserted between AvrII/AscI
pCS2653	pCS2631 with MS2-D5 with S spacers inserted between AvrII/AscI
pCS2686	pCS2595 with 2MS2mut inserted between NotI/ApaI
pCS2688	pCS2686 with sTRSVctrl with spacers inserted between AvrII/AscI
pCS2687	pCS2686 with sTRSV with spacers inserted between AvrII/AscI
pCS2690	pCS2686 with MS2-B1 with spacers inserted between AvrII/AscI
pCS2691	pCS2686 with MS2-B2 with spacers inserted between AvrII/AscI
pCS2694	pCS2686 with MS2-B3 with spacers inserted between AvrII/AscI
pCS2695	pCS2686 with MS2-B7 with spacers inserted between AvrII/AscI
pCS2698	pCS2686 with MS2-B10 with spacers inserted between AvrII/AscI

pCS2699	pCS2686 with MS2-B11 with spacers inserted between AvrII/AscI
pCS2692	pCS2686 with MS2-C1 with spacers inserted between AvrII/AscI
pCS2693	pCS2686 with MS2-C3 with spacers inserted between AvrII/AscI
pCS2697	pCS2686 with MS2-C4 with spacers inserted between AvrII/AscI
pCS2696	pCS2686 with MS2-D5 with S spacers inserted between AvrII/AscI
pCS2747	pCS2595 with NLS-2MS2mut inserted between NotI/ApaI
pCS2749	pCS2747 with sTRSVctrl with spacers inserted between AvrII/AscI
pCS2748	pCS2747 with sTRSV with spacers inserted between AvrII/AscI
pCS2750	pCS2747 with MS2-B1 with spacers inserted between AvrII/AscI
pCS2751	pCS2747 with MS2-B2 with spacers inserted between AvrII/AscI
pCS2758	pCS2747 with MS2-B11 with spacers inserted between AvrII/AscI
pCS2752	pCS2747 with MS2-C1 with spacers inserted between AvrII/AscI
pCS2753	pCS2747 with MS2-C3 with spacers inserted between AvrII/AscI
pCS2759	pCS2747 with MS2-D5 with S spacers inserted between AvrII/AscI
pCS2787	pCS2595 with 2MS2mut-NES inserted between NotI/ApaI
pCS2789	pCS2787 with sTRSVctrl with spacers inserted between AvrII/AscI
pCS2788	pCS2787 with sTRSV with spacers inserted between AvrII/AscI
pCS2790	pCS2787 with MS2-B1 with spacers inserted between AvrII/AscI
pCS2791	pCS2787 with MS2-B2 with spacers inserted between AvrII/AscI
pCS2798	pCS2787 with MS2-B11 with spacers inserted between AvrII/AscI
pCS2792	pCS2787 with MS2-C1 with spacers inserted between AvrII/AscI
pCS2793	pCS2787 with MS2-C3 with spacers inserted between AvrII/AscI
pCS2799	pCS2787 with MS2-D5 with S spacers inserted between AvrII/AscI
pCS2897	pCS2595 with 2MS2mut-DsRedMonomer

pCS2899	pCS2897 with sTRSVctrl with spacers inserted between AvrII/AscI
pCS2898	pCS2897 with sTRSV with spacers inserted between AvrII/AscI
pCS2901	pCS2897 with MS2-B11 with spacers inserted between AvrII/AscI
pCS2900	pCS2897 with MS2-C1 with spacers inserted between AvrII/AscI
pCS2902	pCS2595 with NLS-2MS2mut-DsRedMonomer
pCS2904	pCS2902 with sTRSVctrl with spacers inserted between AvrII/AscI
pCS2903	pCS2902 with sTRSV with spacers inserted between AvrII/AscI
pCS2906	pCS2902 with MS2-B11 with spacers inserted between AvrII/AscI
pCS2905	pCS2902 with MS2-C1 with spacers inserted between AvrII/AscI
pCS2907	pCS2595 with 2MS2mut-DsRedMonomer-NES
pCS2909	pCS2907 with sTRSVctrl with spacers inserted between AvrII/AscI
pCS2908	pCS2907 with sTRSV with spacers inserted between AvrII/AscI
pCS2911	pCS2907 with MS2-B11 with spacers inserted between AvrII/AscI
pCS2910	pCS2907 with MS2-C1 with spacers inserted between AvrII/AscI
pCS1576	pcDNA3.1(+) with DsRed-Express
pCS2391	pCS2595 with EF1α-Clover inserted between BglII/AvrII
pCS2847	pCS2595 with PP7 inserted between NotI/ApaI
pCS2847+sTRSVctrl	pCS2847 with sTRSVctrl with spacers inserted between AvrII/AscI
pCS2847+sTRSV	pCS2847 with sTRSV with spacers inserted between AvrII/AscI
pCS2847+PP7-1	pCS2847 with PP7-1 with spacers inserted between AvrII/AscI
pCS2847+PP7-2	pCS2847 with PP7-2 with spacers inserted between AvrII/AscI
pCS2847+PP7-3	pCS2847 with PP7-3 with spacers inserted between AvrII/AscI
pCS2816	pCS2595 with lambda N inserted between NotI/ApaI
pCS2816+sTRSVctrl	pCS2816 with sTRSVctrl with spacers inserted between AvrII/AscI
pCS2816+sTRSV	pCS2816 with sTRSV with spacers inserted between AvrII/AscI
pCS2816+Lambda-1	pCS2816 with Lambda-1 with spacers inserted between AvrII/AscI

pCS2816+Lambda-2	pCS2816 with Lambda-2 with spacers inserted between AvrII/AscI
pCS2816+Lambda-3	pCS2816 with Lambda-3 with spacers inserted between AvrII/AscI
pCS2816+Lambda-4	pCS2816 with Lambda-4 with spacers inserted between AvrII/AscI
pCS2397	pCS2595 with insertNA inserted between NotI/ApaI
pCS2666	pCS2397 with sTRSVctrl with spacers inserted between AvrII/AscI
pCS2665	pCS2397 with sTRSV with spacers inserted between AvrII/AscI
pCS2672	pCS2397 with p50-1 with spacers inserted between AvrII/AscI
pCS2673	pCS2397 with p50-2 with spacers inserted between AvrII/AscI
pCS2674	pCS2397 with p50-3 with spacers inserted between AvrII/AscI
pCS2675	pCS2397 with p50-4 with spacers inserted between AvrII/AscI
pCS2676	pCS2397 with p50-5 with spacers inserted between AvrII/AscI
pCS2677	pCS2397 with p50-6 with spacers inserted between AvrII/AscI
pCS2668	pCS2397 with p50-7 with spacers inserted between AvrII/AscI
pCS2669	pCS2397 with p50-8 with spacers inserted between AvrII/AscI
pCS2670	pCS2397 with p50-9 with spacers inserted between AvrII/AscI
pCS2671	pCS2397 with p50-10 with spacers inserted between AvrII/AscI
pCS2683	pCS2397 with p50-11 with spacers inserted between AvrII/AscI
pCS2684	pCS2397 with p50-12 with spacers inserted between AvrII/AscI
pCS2685	pCS2397 with p50-13 with spacers inserted between AvrII/AscI
pCS2682	pCS2397 with p65-1 with spacers inserted between AvrII/AscI
pCS2678	pCS2397 with p65-2 with spacers inserted between AvrII/AscI
pCS2679	pCS2397 with p65-3 with spacers inserted between AvrII/AscI
pCS2680	pCS2397 with p65-4 with spacers inserted between AvrII/AscI
pCS2681	pCS2397 with p65-5 with spacers inserted between AvrII/AscI
pCS2604	pCS2391 with p50 inserted between NotI/ApaI
pCS2605	pCS2391 with p65 inserted between NotI/ApaI
pCS2766	pCS2397 with Bcat-A1 with spacers inserted between AvrII/AscI
pCS2767	pCS2397 with Bcat-A2 with spacers inserted between AvrII/AscI
pCS2768	pCS2397 with Bcat-A3 with spacers inserted between AvrII/AscI
pCS2769	pCS2397 with Bcat-A4 with spacers inserted between AvrII/AscI

pCS2397+Bcat-B1	pCS2397 with Bcat-B1 with S spacers inserted between AvrII/AscI
pCS2397+Bcat-B2	pCS2397 with Bcat-B2 with S spacers inserted between AvrII/AscI
pCS2397+Bcat-B3	pCS2397 with Bcat-B3 with S spacers inserted between AvrII/AscI
pCS2397+Bcat-B4	pCS2397 with Bcat-B4 with S spacers inserted between AvrII/AscI
pCS2397+Bcat-B5	pCS2397 with Bcat-B5 with S spacers inserted between AvrII/AscI
pCS2397+Bcat-B6	pCS2397 with Bcat-B6 with S spacers inserted between AvrII/AscI
pCS2824	pCS2595 with β-catenin Arm 1-12 inserted between NotI/ApaI
pCS2850	pCS2824 with sTRSVctrl with spacers inserted between AvrII/AscI
pCS2849	pCS2824 with sTRSV with spacers inserted between AvrII/AscI
pCS2824+Bcat-A1	pCS2824 with Bcat-A1 with spacers inserted between AvrII/AscI
pCS2824+Bcat-A2	pCS2824 with Bcat-A2 with spacers inserted between AvrII/AscI
pCS2824+Bcat-A3	pCS2824 with Bcat-A3 with spacers inserted between AvrII/AscI
pCS2848	pCS2824 with Bcat-A4 with spacers inserted between AvrII/AscI
pCS2824+Bcat-B1	pCS2824 with Bcat-B1 with S spacers inserted between AvrII/AscI
pCS2824+Bcat-B2	pCS2824 with Bcat-B2 with S spacers inserted between AvrII/AscI
pCS2824+Bcat-B3	pCS2824 with Bcat-B3 with S spacers inserted between AvrII/AscI
pCS2824+Bcat-B4	pCS2824 with Bcat-B4 with S spacers inserted between AvrII/AscI
pCS2824+Bcat-B5	pCS2824 with Bcat-B5 with S spacers inserted between AvrII/AscI
pCS2824+Bcat-B6	pCS2824 with Bcat-B6 with S spacers inserted between AvrII/AscI

Supplementary Table 3.5. Human cell lines with stably integrated constructs.

Parental line	Integrated plasmid construct
Flp-In T-REx HEK293	pCS2359
Flp-In T-REx HEK293	pCS2380
Flp-In T-REx HEK293	pCS2381
Flp-In T-REx HEK293	pCS2382
Flp-In T-REx HEK293	pCS2383
Flp-In T-REx HEK293	EF1α-GFP (Ryan Bloom)
Flp-In HEK293	pCS2585 (Melina Mathur)
Flp-In T-REx HEK293	pCS2595
Flp-In T-REx HEK293	pCS2686
Flp-In T-REx HEK293	pCS2688
Flp-In T-REx HEK293	pCS2699
Flp-In T-REx HEK293	pCS2692
Flp-In T-REx HEK293	pCS2693
Flp-In T-REx HEK293	pCS2696
Flp-In T-REx HEK293	pCS2747
Flp-In T-REx HEK293	pCS2749
Flp-In T-REx HEK293	pCS2758
Flp-In T-REx HEK293	pCS2752
Flp-In T-REx HEK293	pCS2753
Flp-In T-REx HEK293	pCS2759
Flp-In T-REx HEK293	pCS2787
Flp-In T-REx HEK293	pCS2789
Flp-In T-REx HEK293	pCS2798
Flp-In T-REx HEK293	pCS2792
Flp-In T-REx HEK293	pCS2793
Flp-In T-REx HEK293	pCS2799
Flp-In T-REx HEK293	pCS2899
Flp-In T-REx HEK293	pCS2898
Flp-In T-REx HEK293	pCS2901
Flp-In T-REx HEK293	pCS2900
Flp-In T-REx HEK293	pCS2904
Flp-In T-REx HEK293	pCS2903
Flp-In T-REx HEK293	pCS2906
Flp-In T-REx HEK293	pCS2905
Flp-In T-REx HEK293	pCS2909
Flp-In T-REx HEK293	pCS2908
Flp-In T-REx HEK293	pCS2911

Flp-In T-REx HEK293	pCS2910
Flp-In T-REx HEK293	pCS2824
Flp-In T-REx HEK293	pCS2850
Flp-In T-REx HEK293	pCS2849
Flp-In T-REx HEK293	pCS2848

Supplementary Table 3.6. Alternate names of RNA devices.

RNA device	Name in notebooks
MS2-A1	LI AU
MS2-A2	LI CU
MS2-A3	LII UG
MS2-A4	LII UG CtoG
MS2-A5	LII UG a1
MS2-A6	LII UG a14
MS2-A7	LII GA
MS2-B1	D1
MS2-B2	D2
MS2-B2ctrl	D2ctrl
MS2-B3	D7
MS2-B4	L81
MS2-B5	L83
MS2-B6	L84
MS2-B7	L85
MS2-B8	L61
MS2-B9	L41
MS2-B10	D7-a1
MS2-B11	L85-a1
MS2-C1	D3
MS2-C1ctrl	D3ctrl
MS2-C2	D4
MS2-C3	D5
MS2-C3ctrl	D5ctrl
MS2-C4	D6
MS2-D1	J1
MS2-D2	J2

RNA device	Name in notebooks
PP7-3	PP7-3
Lambda-1	L2b8-a1-lambda
Lambda-2	L85-a1-lambda
Lambda-3	lambda-4
Lambda-4	lambda-5
p50-1	p50-OFF1
p50-2	p50-OFF1-a1
p50-3	p50-OFF2
p50-4	p50-OFF2-a1
p50-5	p50-OFF3
p50-6	p50-OFF3-a1
p50-7	p50-ON1
p50-8	p50-ON1-a1
p50-9	p50-ON2
p50-10	p50-ON2-a1
p50-11	U12N11
p50-12	U1N1
p50-13	U11N11
p65-1	p65-OFF1
p65-2	p65-ON1
p65-3	p65-ON1-a1
p65-4	p65-ON2
p65-5	p65-ON2-a1
Bcat-A1	Bcat-sLTSV-
Bcat-A2	Bcat-sLTSV+
Bcat-A3	Bcat-CChMVd-
Bcat-A4	Bcat-SCMoV+

MS2-D3	J3
MS2-D4	J4
MS2-D5	J5
MS2-D6	J6
PP7-1	D5-PP7
PP7-2	PP7-2

Bcat-B1	Bcat-OFF3
Bcat-B2	Bcat-OFF4
Bcat-B3	Bcat-OFF5
Bcat-B4	Bcat-OFF6
Bcat-B5	Bcat-ON3
Bcat-B6	Bcat-ON4